NOVEL CONCEPTUAL DESIGN AND ANLYSIS OF POLYMER DERIVED CERAMIC MEMS SENSORS FOR GAS TURBINE ENVIRONMENT

by

NARASIMHA RAJU NAGAIAH
B.S. Bapuji Institute Engineering and Technology,
Kuvempu University, India - 2000

A thesis submitted in partial fulfillment of the requirements
for the degree of Master of Science
in the Department of Mechanical, Materials, and Aerospace Engineering
in the College of Engineering and Computer Science
at the University of Central Florida
Orlando, Florida

Summer Term
2006

ABSTRACT

Technical challenges for developing micro sensors for Ultra High Temperature and turbine applications lie in that the sensors have to survive extremely harsh working conditions that exist when converting fuel to energy. These conditions include high temperatures (500-1500°C), elevated pressures (200-400 psi), pressure oscillations, corrosive environments (oxidizing conditions, gaseous alkali, and water vapors), surface coating or fouling, and high particulate loading. Several technologies are currently underdeveloped for measuring these parameters in turbine engines. One of them is an optical-based non-contact technology. However, these nondirective measuring technologies lack the necessary accuracy, at least at present state. An alternative way to measure these parameters without disturbing the working environments is using MEMS type sensors. Currently, the techniques under development for such harsh environment applications are silicon carbide (SiC) and silicon nitrite (Si_3N_4) –based ceramic MEMS sensors. But those technologies present some limitation such as narrow processing method, high cost (materials and processing cost), and limited using temperatures (typically < 800 ^oC).

In this research we propose to develop two sensors based on recently developed polymer-derived ceramics (PDCs): *Constant Temperature Hot wire Anemometer, temperature/heat-flux sensor for turbine applications*. PDC is a new class of high temperature ceramics. As we shall describe below, many unique features of PDCs make them particularly suitable for the proposed sensors, including: excellent thermo-mechanical properties at high temperatures, enable high temperature operation of the devices; various well-developed processing technologies, such as injection molding, photolithography, embossing, DRIE etching and precise machining, can be

used for the fabrication of the devices; and tunable electric conductivity, enable the proposed sensors fabricated from similar materials, thus reliability considerations associated with thermal mismatch, which is a big concern when using MEMS-based sensors at elevated temperatures, will be minimized.

To My Parents, Fiancé and Friends

ACKNOWLEDGMENTS

I would like to thank all people who played a very important role in my success at graduate studies and research thereby helping me develop intellectually and professionally. First, I want to express my heartily thanks to my academic advisor Dr. Jayanta Kapat, for his initiation of this novel research and valuable guidance to make things happen. Personally I learned lot from him. I want to show my appreciation to my Co-advisor Dr. Linan An, for being patient with my questions arising out of ignorance and also for helping me gain an understanding of material science part of my research. I also want to thank Dr. Quanfang Chen for being my committee member for my defense. I am greatly thankful to my project group at Center for Advanced Turbines and Energy Research (CATER), especially Vaidy, for being with me always and helping me with my research and my academics. I also want to thank my friends Krishna and Umit for their moral support.

I also want to thank International Services Center at UCF for supporting me financially from the beginning. Also I would like to thank two very special people; my parents for making great sacrifices to enable me pursue my dreams. I am forever in debt to them for everything they have done for me. Lastly I cherish the encouragement I got from my Fiancé to complete my thesis on time.

TABLE OF CONTENTS

LIST OF FIGURES

LIST OF TABLES

LIST OF ACRONYMS/ABBREVIATIONS

α	Temperature coefficient of resistance
T	Temperature (K)
ρ	Density (kg/m^3)
k	Thermal Conductivity (W/m. K)
k_{sensor}	Thermal Conductivity of sensor
$k_{substrate}$	Thermal Conductivity of substrate
k_f	Thermal conductivity of fluid
μ	Viscosity
A_w	Wire surface area
h	Heat Transfer Coefficient ($W/m^2.K$)
T_w	wire temperature
T_0	Flow temperature
U	Velocity
U_{eff}	Effective cooling velocity
σ	Specific resistivity
R	resistance
CP	Specific Heat at constant Pressure
Cv	Specific Heat at constant Volume
γ	Gas constant $\equiv$ Cp/Cv
δ	Thickness or distance between two points
ΔT	Change in Temperature between two points

Δt	Change in time between two timesteps
I	Current
V	Voltage
P	Power
D	Diameter
Nu	Nusselt number
Re	Reynolds number
Pr	Prandtl number
M	Amplitude ratio
f	Frequency
τ	Time constant
q"	Heat Flux
Q	Heat transfer rate
ϕ	Heat transfer rate by convection
F_o	Fourier Number $\equiv \alpha \Delta t$

CHAPTER 1
INTRODUCTION

The development of smart materials and sensors has been challenging for some structures, such as gas turbine engines and space crafts, because they operate at extreme conditions of temperature and pressure. Direct measurement of significant hot gas flow parameters and properties, like, velocity, turbulence levels, pressure fluctuations and temperature/heat flux at the exit of a gas turbine combustor or inlet to the first row of vanes or nozzles under actual operating conditions is quite difficult, if not downright impossible, with the currently available measurement tools. Temperatures at that location can be in excess of 1800°K, and the chemical condition can be quite hostile, rendering any off-the-shelf intrusive probe quite useless. Also, for space and geometric restrictions, optical windows (for transmitting and receiving optics) are difficult to be implemented. As a result, conventional optical measurement techniques for measurement of various velocity, turbulence, temperature and species such as Laser Doppler Anemometry (LDV), Particle Image Velocimetry (PIV), and Laser Induced Fluorescence (LIF) cannot be used readily without modifications. As a result, current turbine design primarily relies on estimated or computed data (obtained from CFD simulations, the very basis of which is questionable under these conditions). Yet the flow conditions at that location are very important for turbine design, as they form the inlet boundary conditions for turbine design process.

To improve the working performance and reduce pollution of turbine engines, robust sensing systems are needed for measuring and monitoring physical parameters. The real-time monitoring of flow parameters, like velocity, turbulence levels, flow patterns and temperature profiles/heat flux across a flow section is essential for an overall design optimization of a gas

turbine engine and for precise control. For example, maintaining a high turbine inlet temperature (TIT) is needed for achieving a high thermal efficiency. For the current gas turbines, the hot gas temperatures are already a few hundred degrees hotter than what the metals on the hot-gas-path can take. These metal components can survive only because of advanced cooling techniques and complex ceramic coatings. Thus achieving high efficiency (which corresponds to cheaper electricity) is a delicate and complicated balance of maintaining the gas and metal temperatures within a narrow range. As can be seen from Figure 1, each 100°C increase in TIT results in about 1 percentage point increase in the net efficiency for a simple cycle gas turbine plant.

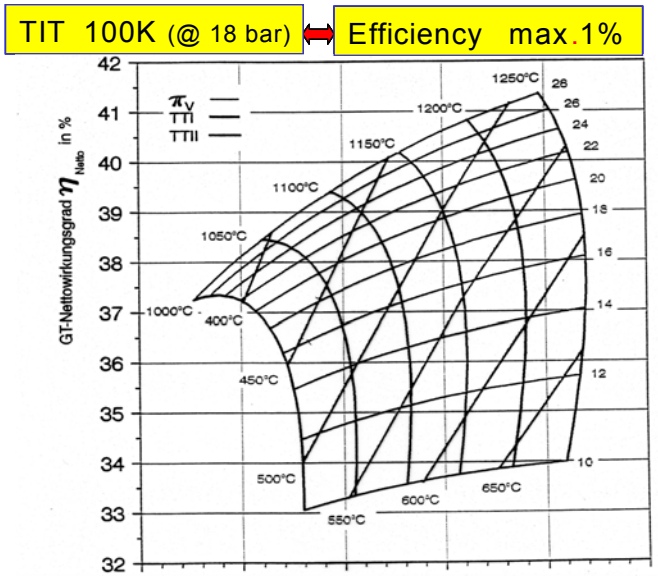

- For life prediction of parts, a temperature variation of **+30K** gives a reduction of life **by a factor of two** .
- For life prediction of parts, to have a life prediction accuracy of **±10%,** the metal temperature needs to be known with an accuracy of **± 4K** and the heat flux with **±1%.**
- For heat transfer, the accuracy of tests that he reported was at best **± 8%.**

Figure 1: Net efficiency vs. Net power as a function of turbine inlet temperature

Furthermore, actual cost to the electricity customer is also dependent on the reliability of the machines. A temperature variation of 30°C gives a reduction in life a factor of 2. In other words, in order to have life prediction accuracy of +/- 10%, one must have an accuracy of +/- 4 °C in knowing metal temperatures and +/- 1% in knowing heat flux. In contrast, the typical

laboratory tests have an uncertainty of +/- 8% in heat transfer correlations. The life of the hot-gas-path parts is further adversely affected by gas stream pressure/temperature and velocity fluctuations, which are not accurately known currently. The lack of accurate predictive capability necessary for ultra-long life necessitates on-line measurement/monitoring of the key process variables such as metal temperature and heat flux, gas path velocity/temperature fluctuations. Even for design validation designer would like to know some of these variables more accurately than what is available today.

The issue becomes even more important for newer power generation concepts such as clean coal technology and Integrated Gasification Combined Cycle (IGCC) plants. Technical challenges for developing sensors for power generation gas-turbine applications lay in that the sensors have to survive extremely harsh working conditions that exist when converting fossil fuel to energy, and the sensors cannot alter the flow field. The harsh working conditions include high temperatures (500-1800°C), elevated pressures (200-600 psi), pressure oscillations, corrosive environments (oxidizing conditions, gaseous alkali, and water vapors), surface coating or fouling, and high particulate loading. Several technologies are currently under development for measuring these parameters in turbine engines. One of them is an optical-based non-contact technology. However, these non intrusive measuring technologies lack the necessary accuracy, at least at present state. An alternative way to measure these parameters without disturbing the working environments is using MEMS type sensors. Currently, the techniques under development for such harsh environment applications are silicon carbide (SiC) and silicon nitrite (Si_3N_4) –based ceramic MEMS sensors. But those technologies present some limitation such as

narrow processing method, high cost (materials and processing cost), and limited using temperatures (typically < 800 ^{o}C).

Consequently, new materials and technologies are desired for gas-turbine sensors. Materials that can be used for making micro-sensors for gas turbine applications will have to meet at least following specifications:

(i) Excellent thermo-mechanical properties to survive the harsh working environments,

(ii) Well-behaved high-temperature electronic properties to obtain reliable signals, and

(iii) Ease in micro-fabrication.

The present research is intended to develop sensors for measurement of velocity, turbulence levels and temperature/heat flux at a high resolution, capable to withstand hostile high temperature flows with direct application to the gas turbine environment. The fundamental approaches to sensor-material combination that builds upon advancement in materials, development in miniature sensors. These sensors are to be fabricated using indigenously developed Polymer Derived Ceramics (PDCs) with overall dimensions to enable measurements at a higher resolution which can be placed on a hot gas path wall (such as at combustor exit/ turbine inlet), perhaps in a line around circumference, and that can continuously monitor velocity, turbulence levels and temperature/heat flux. Figure 2, shows sectional view of Industrial Gas turbine along with blown up section of combustion chamber and turbine inlet which is our region of interest to measure the flow parameters.

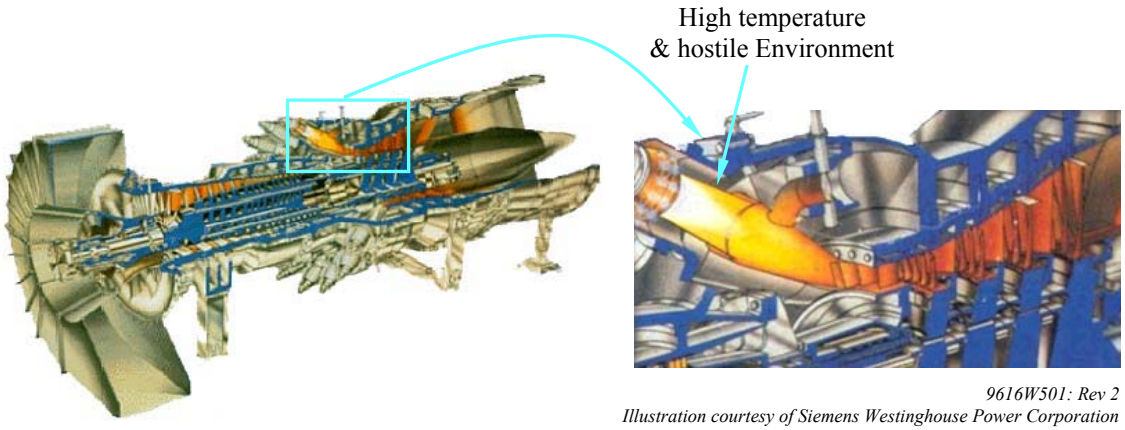

9616W501: Rev 2
Illustration courtesy of Siemens Westinghouse Power Corporation

Figure 2: Sectional view of industrial gas turbine

CHAPTER 2
LITERATURE REVIEW

2.1 Hot Wire Anemometer (HWA):

Comte-Bellot [1]. noted that the precise origin of hot-wire anemometry cannot be accurately determined. One of the earlier studies of heat transfer from a heated wire was made by Boussinesq [2] in 1905. The results obtained by Boussinesq were extended by King [3] and he attempted to experimentally verify his theoretical results. These earlier investigations of hot-wire anemometry considered only the mean heat transfer characteristics from heated wires. The first quantitative measurements of fluctuations in subsonic incompressible flows were made in 1929 by Dryden and Kuethe [4] using constant current anemometry where the frequency response of the wire was extended by the use of a compensating amplifier. In 1934 Ziegler [5] developed a constant temperature anemometer for measuring fluctuations by using a feedback amplifier to maintain a constant wire temperature up to a given frequency.

In the 1950's, Kovasznay [6, 7] extended hotwire anemometry to compressible flows where it was found experimentally that in supersonic flow the heated wire was sensitive only to mass flow and total temperature. Kovasznay developed a graphical technique to obtain these fluctuations, which is mostly used in supersonic flow. In subsonic compressible flows the heat transfer from a wire is a function of velocity, density, total temperature, and wire temperature. Because of this complexity, these flow regimes were largely bypassed until the 1970's and 1980's

when attempts were made to develop methods applicable [8] for these flows. In recent years there were several new and promising developments in hot-wire anemometry that can be attributed to advances in Fabrication techniques (MEMS), electronics, data acquisition/reduction methods and new developments in basic anemometry techniques.

Conventional HWAs are assembled individually by mounting a thin wire made of platinum, tungsten or platinum-iridium (80% pt, 20% Ir) [9], on to support shanks. The wires may be thinned (e.g., by etching in acidic solutions) until the desired dimensions are reached, typically a few mm long and a few micrometers in diameter, this active portion of the sensor is then mounted on a long probe with electrical connection for ease of handling. The conventional HWA is noted for its low cost, fast response, small size and low noise [9]. However these HWAs pose significant problems in gas turbine environment where the high-speed flow and ultra high temperature are common. Therefore these HWAs are not suitable for hostile environments, such as combustion [10].

In the past two decades, several research groups have developed micromachined flow sensors that are based on a variety of sensing principles including thermal anemometry. Microfabrication offers the benefits of high spatial resolution and fast time response (due to low thermal mass).

Jiang et al. [11]. Have reported recently making micromachined Hot-Wire Anemometers, where the prongs and hot-wires are out of doped polycrystalline silicon. They showed The systematic characterization of these devices, especially of the steady-state characteristics,

frequency response, and directional dependence. Also showed these micromachined anemometers can perform better than conventional ones because of their extremely small size. It is demonstrated that a 10 mm long, 1 mm wide, and 0.5 mm thick polysilicon hot wire can have a unprecedented bandwidth of 1.4 MHz in constant-temperature mode.

Chen et al. [12]. reported the development of a new type of hot-wire anemometer (HWA) realized by using a microfabrication process that combines surface micromachining and an efficient three-dimensional assembly technique. The HWA uses a thermal element (hot wire) that is made of Pt/Ni/Pt film with a measured temperature coefficient of resistance (TCR) of 2400 ppm/ C. The thermal element is elevated out of plane by using support beams made of polyimide. In their current design, the support beam is 2.7 m thick and up to 1 mm tall, and the length of the thermal element varies from 50 mto 200 m. Steady-state response to air velocity has been experimentally obtained up to 20 m/s under both constant current (CC) and constant temperature (CT) modes. The transient-state response has been examined using square wave and sinusoidal wave excitation signals in CT modes with the maximum cutoff frequency found to be approximately 10 kHz. This new HWA claim to be offering number of unique materials and performance characteristics.

Ebefors et al. [13]. used doped silicon for both the prong and the hot-wire along with polyamide hinges to make the first three-component (3-D) hot-wire sensors based on polymide joints. Their new 3-D HWA is specially designed for turbulent gas flow measurements. The sensor probe consists of three perpendicular 500μm x 5μm x 2μm polysilicon hot-wires giving a measuring volume sufficiently small to resolve the small eddies in a turbulent flow. A bulk

micromachining process in combination with sacrificial etching is used to form the hot-wire probes. The hot-wires are connected to 30μm thick bulk silicon beams which are defined by double sided KOH etching. Two wires (*x* and *y*) are located in the wafer plane and the third z-wire is rotated out of the plane using a new robust micro-joint. The self-assembly micro-joint with small bending radius is based on thermal shrinkage of polyimide in V-grooves. High flow sensitivity for the anemometric hot-wires has been measured. Time constants of 120 and 330μs were measured for the cooling and heating of the hot-wires, respectively.

Carlsson et al. [14]. showed that all MEMS based hot-wire sensors have the severe drawback of a non-circular cross-section of the wire, and this raised some crucial questions on the accuracy of the determined quantities. To sort out the questions associated with the noncircular cross-section, they conducted simple calibrations of a silicon based hot-wire and compared these results to a conventional hot-wire.

Sherif et al. [15]. studied an analytical procedure for predicting the response of constant temperature hot-wire and film anemometers. His paper introduced a method capable of predicting the constant-temperature anemometer response of any single wire or film probe in a known flow field. The method is also capable of predicting the probe response at any orientation once the response is known at another orientation.

Freymuth [16]. estimated heat conduction loss through prongs in case of conventional HWAs. He presented static and dynamic end conduction losses for constant temperature hot-wire sensors in graphical form and in simple equations. “Side losses’’ for non-cylindrical sensors

according to the Bellhouse-Schultz model are also represented displaying qualitative similarities and quantitative differences of end losses and side losses. In our design we observed significant decrease in end losses due to type of material we are using.

2.2 Heat Flux Sensor (HFS):

Heat flux is one of the important parameters, together with pressure, temperature, velocity, etc., of interest to gas-turbine engine designers. There is need for heat flux sensor that can measure high heat fluxes (~ 1 MW/m^2) at high surface temperature and under large transverse gradients, especially inner walls of combustion chamber in gas turbines.

Limitation of current Heat Flux sensors for gas turbine applications were also discussed by Bennethum et al. [17]. according to their survey, deterioration of the sensor surface due to oxidation was a problem with thin film sensors used in high temperature environments. The requirement of a cold side for the heat flux sensor installation and for routing the leads limit heat flux sensors like the embedded thermocouple gage, Gardon gage, and the slug calorimeter unsuitable for high temperature combustor component measurements.

Paulon et al. [18]. Godefroy et al. [19]. also discuss techniques for high heat flux measurements in turbomachinery, particularly at high temperatures. These two researchers have fabricated thin-film heat flux sensors (< 80 mm) for use in high temperature environments. The sensors were made by forming thin film thermocouple junctions on either side of a Kapton layer. No quantitative data on the performance of the thin film sensors have been presented.

Wrbanek et al. [20]. group at NASA Glenn Research center currently investigating the feasibility of ceramics as thin film thermocouples for extremely high temperature applications to take advantage of the stability and robustness of ceramics and the non-intrusiveness of thin films. They are doing research on fabricating High temperature heat flux sensor using ceramic thermocouples pile. They also stated the use of thin film sensors has several advantages over wire or foil sensors. Thin film sensors do not require special machining of the components on which they are mounted, and, with thicknesses less than 10 μm, they are considerably thinner than wire or foils. Thin film sensors are thus much less disturbing to the operating Environment or flow field, and have a minimal impact on the physical characteristics of the supporting components.

Long et al. [21]. described the design, manufacture, and calibration of two thermopile-types, heat flux sensors: a titanium plug sensor and a ceramic annular sensor. The intended application of both these instruments is on a high rotational speed test rig. The titanium sensor was constructed using eight thermopile junction pairs arranged in radial groves on either side of a 5-mm thickness titanium plug. The annular sensor was constructed from copper-electroplated constantan wire, wound around a 0.5 mm thickness of Macor ring. This ring was then embedded into a titanium plug. The calibrations were carried out under the stagnation point of an impinging jet onto an electrically heated surface. Existing, published Nusselt number correlations were used to provide the expected heat flux and the voltage output of the sensors was measured experimentally.

Neumann et al. [22]. discuss the details of the problems in heat flux measurements encountered during hypersonic testing. Kidd [23], describes some successful heat flux measurement techniques at these high temperature, high heat flux conditions. A review of the standard methods for application to the severe conditions of the gas-turbine found none of the techniques to be sufficient.

CHAPTER 3
POLYMER DERIVED CERAMIC MATERIALS (PDC)

Polymer-Derived Ceramics (PDC) is the common name for a class of ceramics synthesized by thermal decomposition of polymer precursors. PDC processing includes the following basic steps, as shown in Figure 3 [24, 25]:

(i) Synthesize/modify polymer precursors,

(ii) Shape and cross-link to form infusible polymer components, and

(iii) Convert the polymer component to ceramic one by pyrolysis at ~ 1000 ^{0}C.

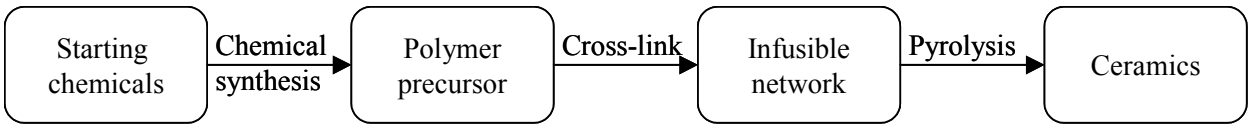

Figure 3: Basic processing steps in polymer-derived ceramics

The materials thus obtained are predominantly amorphous alloys, consisting of silicon, carbon and nitrogen [25]. Other elements such as Boron (B) and Aluminum (Al) can also be incorporated into the network for modifying and improving material properties [26-29].

The PDC materials are particularly suitable for the proposed applications due to their following unique features:

3.1 Excellent thermo-mechanical properties at high temperatures:

While synthesized at relatively low temperatures, the polymer-derived ceramics exhibited excellent high temperature properties:

(i) They resist thermal decomposition and large-scale crystallization up to 1800 ^{o}C Figure 4 [26];

(ii) They possess much better resistance to oxidation and hot-corrosion than CVD SiC and Si_3N_4 (Figure 5, Figure 6 and Figure 7) [30, 31]; and

(iii) Their creep resistance exceeds that of the state-of-the-art polycrystalline SiC and Si_3N_4 [32-34].

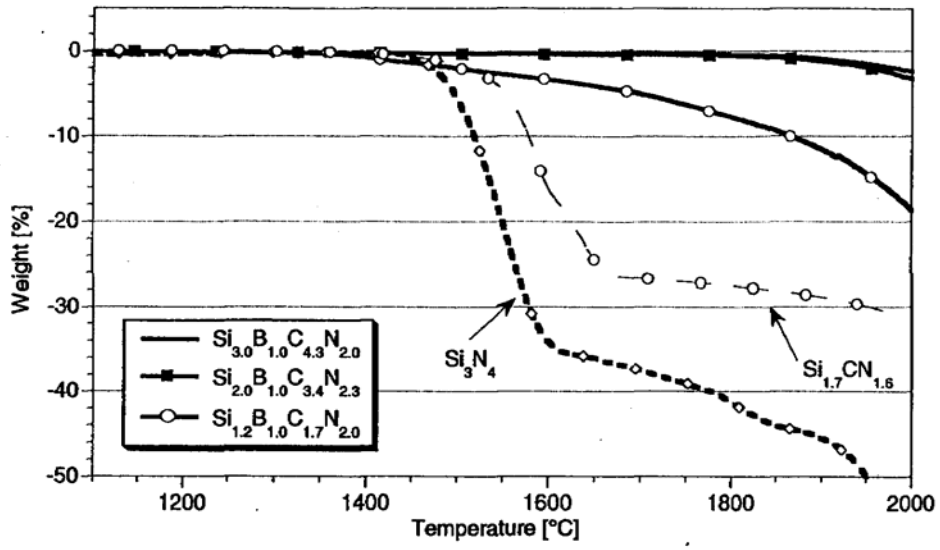

Figure 4: TGA of polymer-derived SiCN, SiBCN and commercial SiN in 0.1MPa He at a heating rate of 5 K/min, suggesting SiBCN can be stable up to 1800 ^{o}C.

Figure 5. Shows a plot of the square of oxide scale thickness as a function of annealing time at 1200 ^{o}C in dry air for SiCN, SiAlCN-07 and SiAlCN-14: SiCN exhibits parabolic behavior; while oxidation rates of the SiAlCN decrease with time at beginning and becomes constant at very low value after ~ 100 hrs to reach a so-called steady-state oxidation stage. The insert table lists the compositions and oxidation rates for different Si-based ceramics. It can be

seen that the steady-state oxidation rate of SiAlCN-14 is an order of magnitude lower than the lowest value of CVD Si_3N_4 and SiC reported previously [35].

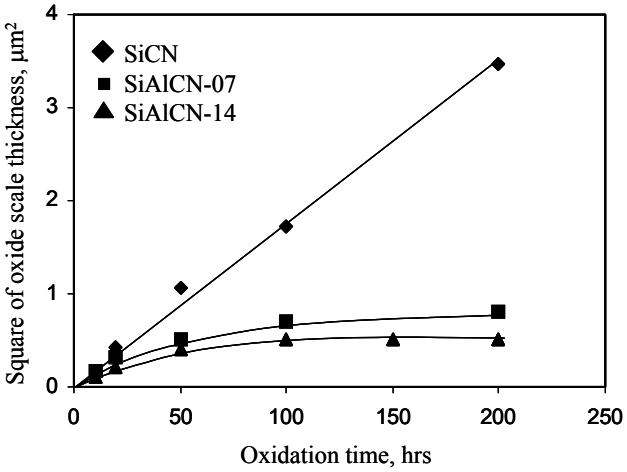

Mats.	Comp.	Kpx10^{18} m^2/sec
SiCN	$SiC_{0.99}N_{0.85}$	4.8
SiAlCN-07	$SiAl_{0.02}C_{0.99}N_{0.85}$	0.3
SiAlCN-14	$SiAl_{0.04}C_{0.83}N_{0.93}$	0.025
CVD SiC	-	0.55
CVD Si_3N_4	-	0.22

Figure 5: A plot of the square of oxide scale thickness as a function of annealing time at 1200 ^{0}C.

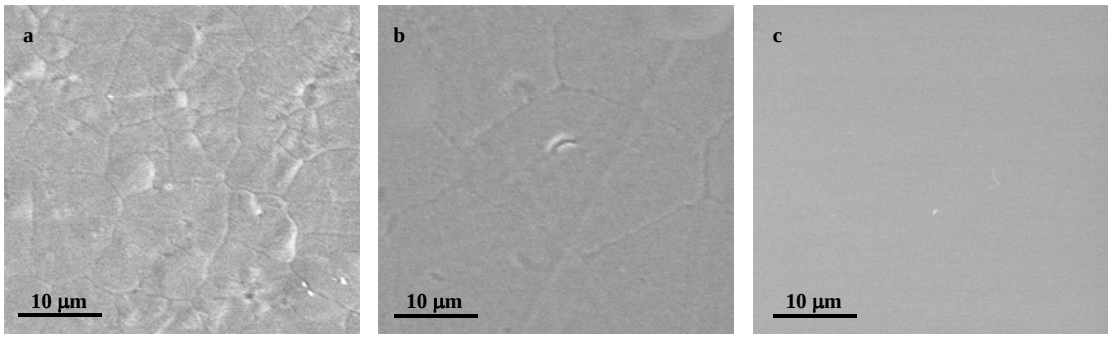

Figure 6: SEM images of the surfaces of (a) SiCN, (b) SiAlCN-07, and (c) SiAlCN-14 after annealing at 1200 ^{o}C for 50 hrs in NaCl environments. SiAlCN-14 shows significant resistance to alkali corrosion without detectable corrosion.

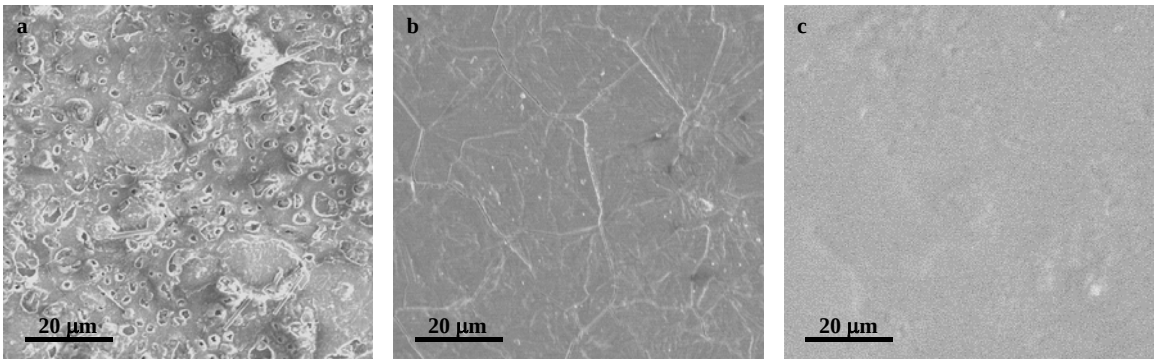

Figure 7: SEM images of the surfaces of (a) SiCN, (b) SiAlCN-07, and (c) SiAlCN -14 after annealing in 100% water vapor of 1 atmosphere pressure at 1200 ^{o}C for 50 hrs. Again, SiAlCN-14 shows excellent resistance to water vapor corrosion without detectable corrosion.

Table 1. Shows some physical-mechanical properties of PDC as compared to the other ceramics (SiC, Si_3N_4). Note that the PDC possess much better thermal shock resistance. Due to the absence of grain boundary phases, it is expected that such excellent mechanical behavior can be retained at high temperatures. These excellent thermo-mechanical properties suggest that the PDCs are suitable for high temperature applications.

Table 1: Properties of polymer derived SiCN and other high temperature materials

Properties	**PDC-SiCN**	**SiC**	**Si_3N_4**
Density (g/cm^3)	2.3	3.17	3.19
Young's modulus (GPa)	90-150	400	320
CTE (x10^{-6}/K)	3	3.8	2.5
Poisson's Ratio	0.18	0.14	0.24
Strength (MPa)	~1000	420	700
Hardness (GPa)	20	30	28
Thermal Shock FOM*	~300	350	880

Thermal shock FOM = strength/(E-young's modulus.CTE)

3.2 Tunable electric conductivity:

The electric conductivity of PDCs can be tailored in a large range [36-38]: from insulator 10^{-8} $(\Omega.cm)^{-1}$ to semi-metallic 10^{4} $(\Omega.cm)^{-1}$. Figure 8. Shows the conductivity of polymer-derived SiAlCN as a function of temperature. It can be seen immediately that the conductivity of this material is perfectly repeatable during heating/cooling cycles up to 1000 ^{0}C, suggesting that the sensors made from the material can be repeatedly used to high temperatures when conductivity is used as sensing mechanism. Figure 8. Also suggests that the SiAlCN material shows typical amorphous semiconductor behavior [39]. The sensitivity of proposed sensor depends on temperature coefficient of resistivity of the sensing material, which can be calculated by:

$$\alpha = \frac{\partial R}{R \partial T} = \frac{B}{T^2} \tag{3.1}$$

For the SiAlCN, α is $4x10^{-3}$ at 600 K, $3x10^{-3}$ at 1000 K and $1.3x10^{-3}$ at 1500 K, in the same range with metal materials (such as Pt, $\alpha = 3x10^{-3}$).

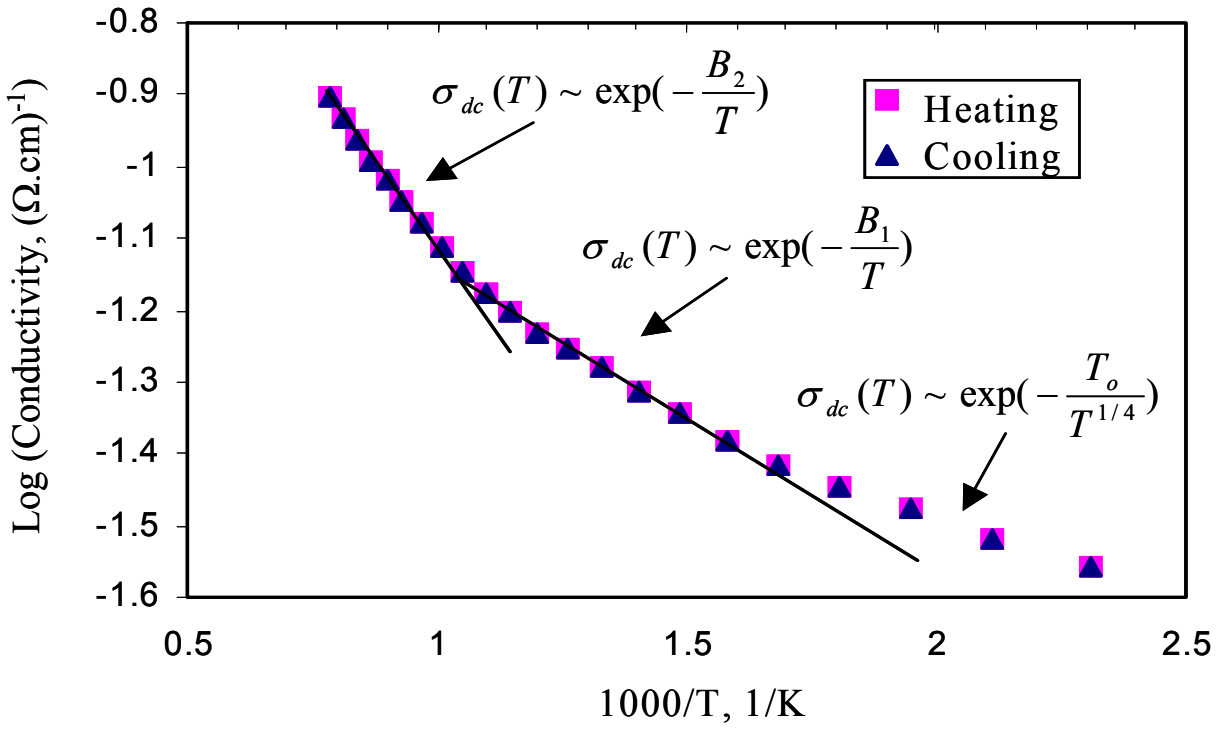

Figure 8: Electric conductivity of SiAlCN as a function of temperature, suggesting amorphous semiconductor behavior of SiAlCN [39].

3.3 Easy for microfabrication:

The direct chemical-to-ceramic processing route of PDCs enables the employment of many well-developed microfabrication technologies. MEMS components and devices can be first made in organic form and then converted to ceramics. Recently, the microfabrication techniques, such as micro-casting, lithography and polymer-based bonding, have been developed for the fabrication of ceramic MEMS with these novel materials [40-45]. Figure 9. Shows some representative PDC MEMS structures.

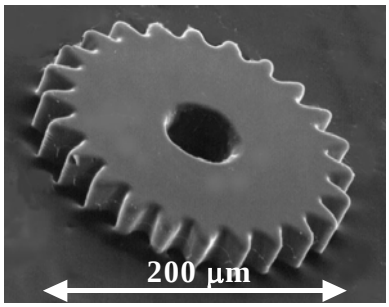

(a)

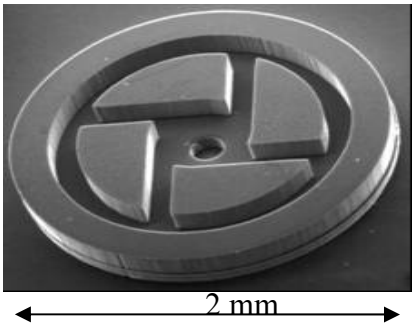

(b)

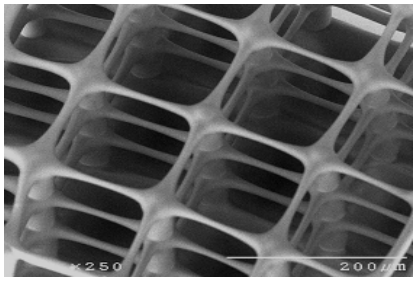

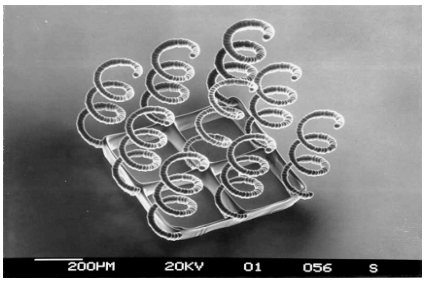

Figure 9: (a) SEM image of SiCN micro-gear fabricated by microinjection molding; (b) Optical image of SiCN atomizer fabricated by lithography; (c) & (d) Ceramic Complex microstructures fabricated by microstereolithography

CHAPTER 4:
POLYMER DERIVED CERAMIC –HOT WIRE ANEMOMETER

4.1 Introduction to Hot Wire Anemometer (HWA):

The hot-wire anemometer (HWA) has been used for many years as a research tool in fluid mechanics. It utilizes a small, electrically heated element exposed to the fluid medium for the purpose of measuring the flow parameters. Normally the parameters being measured are velocity, turbulence levels and flow patterns. The hot-wire anemometer is based on convective heat transfer from a heated element placed in the fluid flow. Any changes in the fluid medium will cause forced convective cooling/heat loss of sensor (wire) [46]. Accordingly, the temperature of the sensor (wire) provides the means to gauging the cooling rate and the flow parameters like velocity and turbulence levels.

Conventional HWA are assembled individually by mounting a thin wire made of platinum or tungsten onto support prongs. The wires may be thinned (e.g., by etching in acidic solutions) until the desired dimensions are reached (typically a few mm long and a few micrometers in diameter). This active portion of the sensor is then mounted on a long probe with electrical connection for ease of handling. The schematic diagram of a typical finished device is shown in Figure 10 the HWA is noted for its low cost, fast response (in the kilohertz range), small sizes, and low noise [46]. Conventional HWAs suffer from two major shortcomings, however. First, the fabrication and assembly process is delicate and does not guarantee uniformity of performance. Secondly, it is prohibitively difficult to form large arrays of HWA for measuring flow distribution.

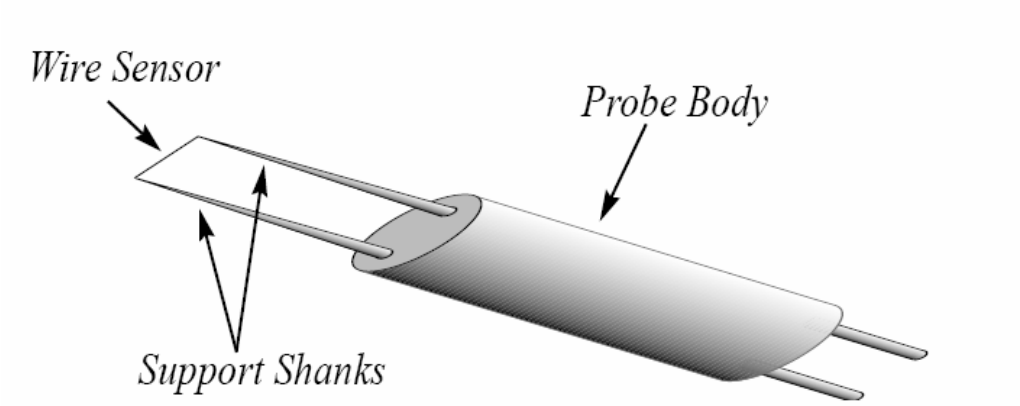

Figure 10: Schematic diagram of a conventional hot-wire anemometer.

4.2 Working Principle of Hot Wire Anemometer

Thermal anemometers measure fluid velocity by sensing the changes in heat transfer from a small, electrically heated element exposed to the fluid. In the "constant temperature anemometer" the cooling effect produced by the flow passing over the element is balanced by the electrical current to the element, so that the element is held at a constant temperature. The change in current due to a change in flow velocity shows up as a voltage at the anemometer output. A modern anemometer will be linked to a personal computer, where the data is analyzed and presented. Figure 11, Shows schematic of electrical circuit and hot wire probe connected to data acquisition system. A key feature of the thermal anemometer is its ability to measure very rapid changes in velocity. This is accomplished by coupling a very fine sensing element (typically a wire four to six microns in diameter or a platinum thin-film deposited on a quartz substrate) with a fast feedback circuit which compensates for the drop in the natural response of the sensor. Time response to flow fluctuations as short as three microseconds can be achieved

easily. It is for this reason the thermal anemometer has become a standard tool for researchers examining the nature of turbulence. The small sensor size, normally only a millimeter in length also makes this technique valuable in applications where access is difficult or where larger sensors obstruct the flow.

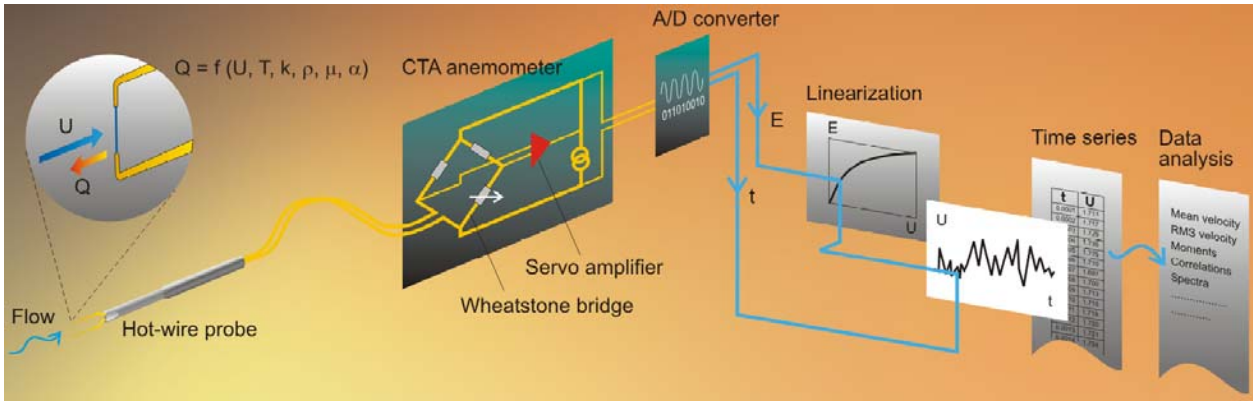

Figure 11: Schematic circuit diagram of CTA Anemometer (Courtesy: Dantec Dynamics)

Convective heat transfer Q from a wire is a function of the velocity U, the wire over-temperature T_w-T_0 and the physical properties (κ, ρ, μ) of the fluid. The basic relation between Q and U for a wire placed normal to the flow was suggested by L.V.King (1914). In its simplest form it reads:

$$Q = (T_w - T_0) A_w h = A + BU^n; \quad n \approx 0.5 \tag{4.1}$$

Where A_w is the wire surface area and h the heat transfer coefficient, which are merged into the calibration constants A and B.

Figure 12, Shows simple Wheatstone bridge circuit for anemometer setup. The sensing wire R_w, is connected to one arm of a Wheatstone bridge and heated by an electrical current. A servo amplifier keeps the bridge in balance by controlling the current to the sensor so that the resistance – and hence temperature – is kept constant, independent of the cooling imposed by the fluid. The bridge voltage, E, represents the heat transfer and is thus a direct measure of the velocity. The combination of the sensor's low thermal inertia and the high gain of the servo loop amplifier give a very fast response to fluctuations in the flow.

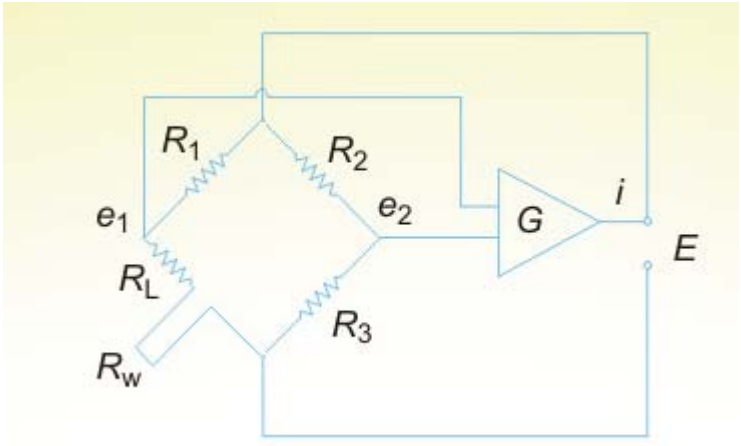

Figure 12: Simple Wheatstone bridge Circuit diagram for anemometer

4.3 Types of Hot-Wire Anemometer Probes /Sensors:

4.3.1 Sensor Types:

Anemometer probes are available with four types of sensors: Miniature wires, Gold-plated wires, Fibre-film or Film-sensors. Wires are normally 5 μm in diameter and 1.2 mm long suspended between two needle-shaped prongs. Gold-plated wires have the same active length but are copper- and gold-plated at the ends to a total length of 3 mm long in order to minimize prong interference. Fibre-sensors are quartz-fibers, normally 70 μm in diameter and with 1.2 mm active length, covered by a nickel thin-film, which again is protected by a quartz coating. Fibre-sensors are mounted on prongs in the same arrays as are wires. Film sensors consist of nickel thin-films deposited on the tip of aerodynamically shaped bodies, wedges or cones.

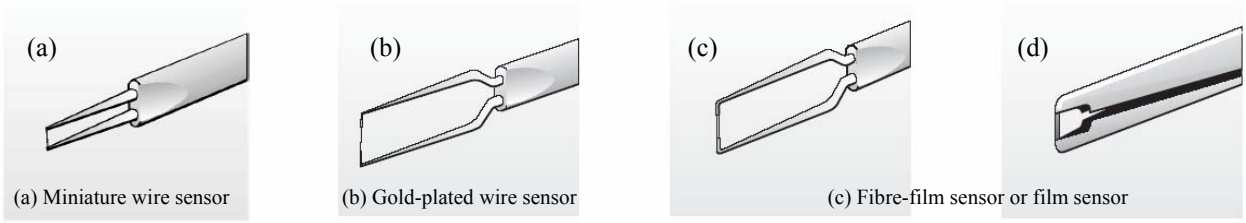

Figure 13: Figure shows sensor types (courtesy: Dantec Dynamics).

4.3.2 Sensor Arrays

Probes are available in one-, two- and three-dimensional versions as single-, dual and triple sensor probes referring to the number of sensors (ref. Figure 14) Since the sensors (wires or fibre-films) respond to both magnitude and direction of the velocity vector, information about both can be obtained, only when two or more sensors are placed under different angles to the flow vector. Split-fibre and triple-split fibre probes are special designs, where two or three thin-film sensors are placed in parallel on the surface of a quartz cylinder. They may supplement Xprobes in two-dimensional flows, when the flow vector exceeds an angle of ±45°.

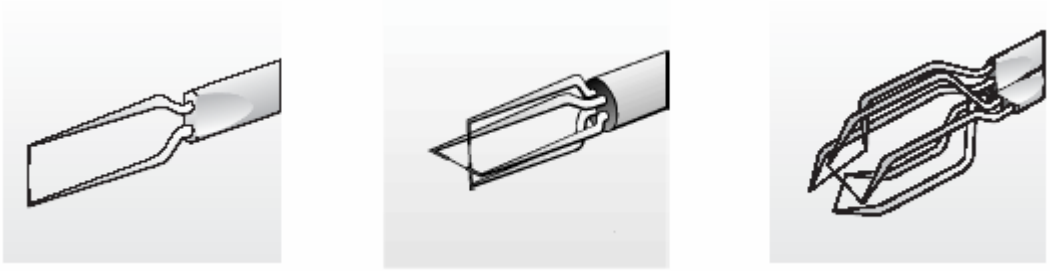

Figure 14: single-, dual and triple sensor probes

4.4 Summary of Technical Data for Conventional HWA.

4.4.1 Sensor material

The standard sensor materials are selected on the basis of the most common applications. The following property values are of importance when selecting sensor material:

To provide high flow sensitivity:	
• High specific resistivity	σ ($\Omega \cdot m$)
• High temperature coefficient of resistance	α (%/K)
To provide small time constant:	
• Small density	ρ (kg/m^3)
• Small heat capacity	c ($J/kg \cdot K$)
To reduce heat transfer to the prongs:	
• Small thermal conductivity	k ($W/m \cdot K$)
To withstand the flow:	
• High tensile strength	γ (N/m^2)
• High resistance against chemical attacks (oxidization)	

Courtesy: Dantec dynamics

As appears from the Table 2 tungsten is a superior sensor material in most applications mainly due to its high mechanical strength.

Table 2: Thermo-Physical properties of materials used in Conventional HWA. (Courtesy: Dantec dynamics)

	Unit	Tung-sten	Pure platinum	PtRh 10% Rh	Pt Ir 20% Ir	Nickel
Resistivity	$\Omega \cdot m \cdot 10^8$	7.0	10.2	18.9	32.0	6.6
Temp. coeff. of res.	$\%/^0C$	0.36	0.38	0.16	0.07	0.64*
Density	$kg/m_3 \cdot 10^{-3}$	19.3	21.45	19.95	21.61	8.9
Heat capacity	$J/kg \cdot K$	33.0	31.4	35.4	32.0	105.0
Heat conductivity	$W/m \cdot K$	178	69.0	50.1	25.5	90.5
Tensile strength	$N/m^2 \cdot 10^{10}$	2.50	0.30	0.60	1.32	0.65
Max. operating temp.	^0C	300	1200	800	700	400
Can be welded		if plated	yes	yes	yes	-
Can be soldered		if plated	yes	yes	yes	yes
Figure of merit	$\Omega \cdot W \cdot 10^9$	4.1	5.7	4.4	3.6	4.5

Courtesy: Dantec dynamics

4.4.2 Sensor resistance

The sensor resistance figures given in the technical data are typical values. The resistance of a sensor depends upon both its dimensions and resistivity of the sensor material. It is expressed as,

$$R = \frac{\rho_r l}{A} \tag{4.2}$$

Where 'ρ_r' is the coefficient of resistivity and 'A' is its cross-sectional area. Also the actual values vary from probe to probe due to manufacturing tolerances. Wire probes have much closer tolerances, normally around ±10%, than film probes, which can vary more than ±50% around the typical value. The film probe resistance is determined not only by the sensor geometry but also by thickness and the metallic structure of the thin film resulting from the sputtering process. Actual sensor resistance is written on the label on the probe container for each individual probe. Sensor resistances are always given at 20°C.

4.4.3 Temperature coefficient of resistance

The relation between resistance and temperature for a metallic conductor can be expressed by means of the temperature coefficient of resistance α_0 (TCR):

$$R_T = R_0 \cdot (1 + \alpha_0 \cdot (T - T_0)) \tag{4.3}$$

Higher order terms are negligible for the normally used sensor materials in a temperature range of a few hundred degrees.

The TCR value α_0 refers to 20°C. The TCR at another temperature T_1 may be calculated as:

$$\alpha_1 = \frac{\alpha_{20}}{(1 + \alpha_{20} \cdot (T_1 - 20))} \tag{4.4}$$

The TCR figure stated for a wire probes is a typical value common for all probes with that wire type. For film probes it may vary with the metal structure and degree of annealing. The TCR is therefore measured for each individual film probe and written on the probe label.

Further the following Table 3 gives summary of other technical data pertaining to HWA.

Table 3: Summary of Technical data for Conventional HWA: (Courtesy: Dantec dynamics)

SENSOR TYPE	Sensor material	Sensor dimensions	Sensor resistance R_{20} (approx.)	Temperature coefficient of resistance (TCR) α_{20} (approx.)	Max. sensor temperature	Min. velocity	Max. velocity	Frequency limit f_{max}(63% response)	Medium
Gold-plated wire sensors	Platinum-plated tungsten	5 µm dia. 1.25 mm long	3.5 Ω	0.36%/K	300°C	0.20 m/s	200 m/s	90 kHz	Air
Miniature wire sensors	Platinum-plated tungsten	15 µm dia. 1.25 mm long	3.5 Ω	0.36%/K	300°C	0.20 m/s	500 m/s	150 kHz	Air
Wire sensors for temperature measurements	Platinum	1 µm dia. 0.4 mm long	50 Ω	0.35%/K	—	—	60 m/s	2 kHz	Air
Fiber-film sensors	Nickel	70 µm dia. 1.25 mm long	6 Ω	0.40%/K	300°C	0.20 m/s	350 m/s	90 kHz	Air
			6 Ω	0.40%/K	150°C	0.01 m/s	10 m/s	30 kHz	Water
Split-fiber sensors	Nickel	200 µm dia. 1.25 mm long	6 Ω	0.40%/K	300°C	0.20 m/s	350 m/s	40 kHz	Air
Wedge-shaped film sensors	Nickel	1 mm × 0.2 mm	15 Ω	0.30%/K	300°C	0.1 m/s	500 m/s	20 kHz	Air
			15 Ω	0.30%/K	150°C	0.01 m/s	25 m/s	30 kHz	Water
Conical film sensors	Nickel	0.75 mm × 0.1 mm	15 Ω	0.35%/K	300°C	0.1 m/s	500 m/s	50 kHz	Air
			15 Ω	0.35%/K	150°C	0.01 m/s	25 m/s	20 kHz	Water
Flush-mounting film sensors	Nickel	0.75 mm × 0.2 mm	15 Ω	0.35%/K	200°C	—	—	—	Air
			15 Ω	0.35%/K	150°C	—	—	—	Water
Glue-on film sensors	Nickel	0.9 mm × 0.1 mm	15 Ω	0.40%/K	200°C	—	—	—	Air

4.5 Design, Specification and Fabrication techniques for PDC-HWA

4.5.1 Design and Specification:

The design and construction of the conventional thermal sensors have limitation in their size as well as strength to withstand hostile environment. They are not suitable for high temperature flows because of their materials construction. Polymer-derived ceramics are proposed here in order to overcome these limitations for measurements of high temperature flows in gas turbines. The conceptual schematic of the proposed sensor is given in Figure 15 all components will be fabricated with polymer-derived ceramics with different conductivities. Such design not only improves the high temperature durability of the sensors due to the use of high temperature materials but also eliminates the thermal mismatch which is one of the main reasons to cause the lose of reliability of devices.

The conceptual design of PDC-HWA is based on conventional HWA. At present the research is focused on testing feasibility of using new material (PDC) in the field of sensor. To start with we considered specifications in proportionate to conventional HWA. Only difference in our design of hot wire anemometer is the wire, which is non-circular in cross section compared to circular cross section in conventional HWA. Figure 15 shows conceptual design of PDC-HWA, also notice non-circular nature of the sensor wire (SiAlCN).

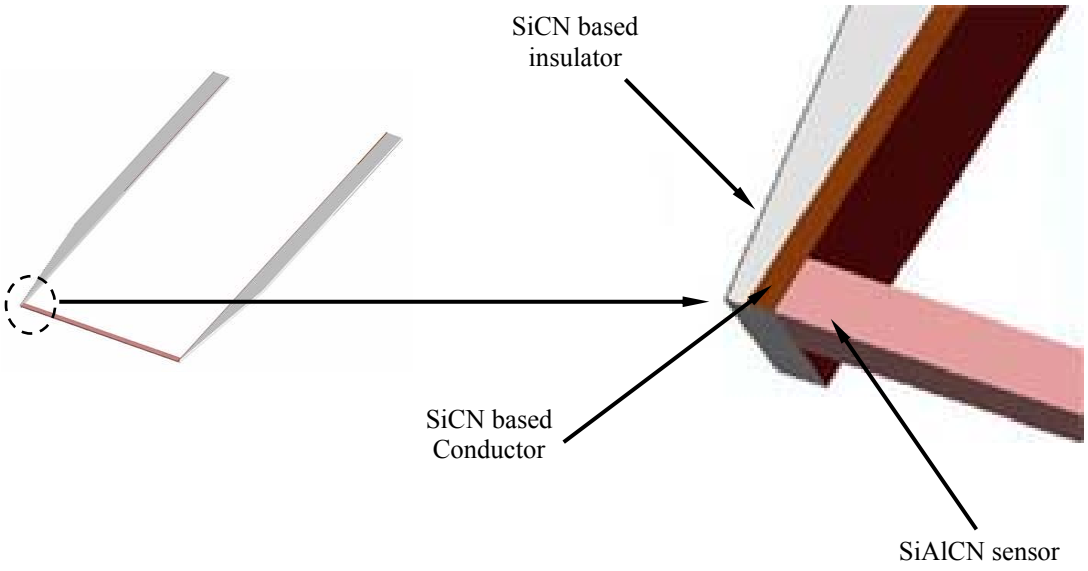

Figure 15: Polymer Derived Ceramic-HWA.

Figure 16 shows specification of PDC-HWA, where as Figure 17, shows different design to incorporate temperature sensing wire with velocity and turbulence sensing wire.

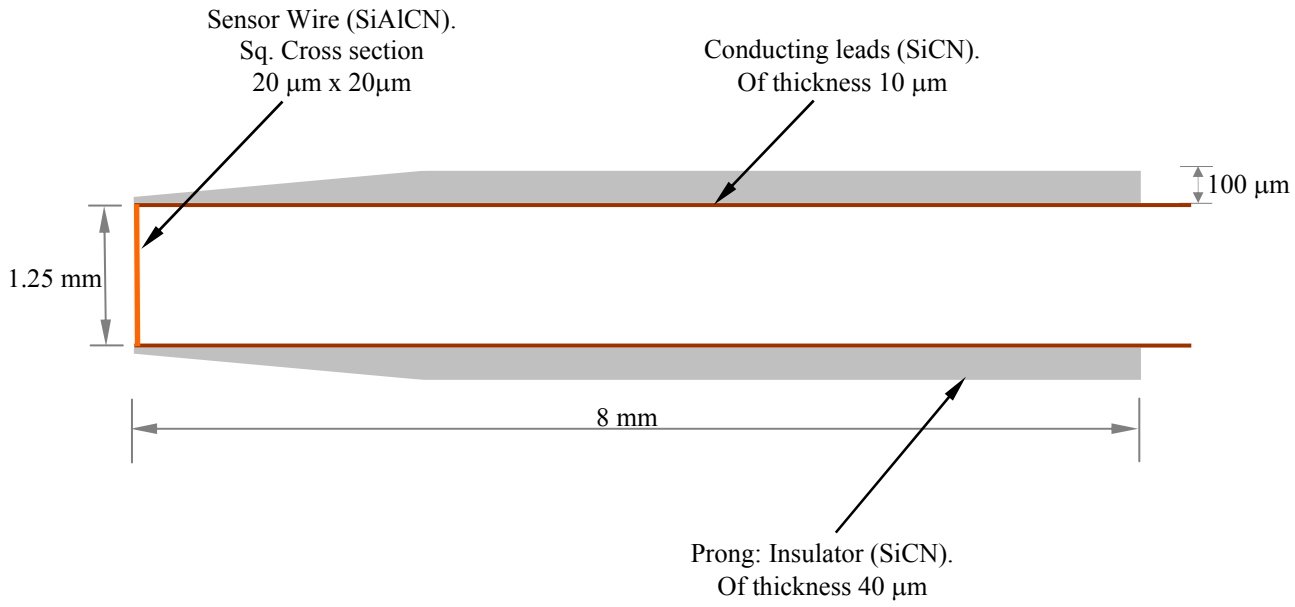

Figure 16: Specification of PDC-HWA

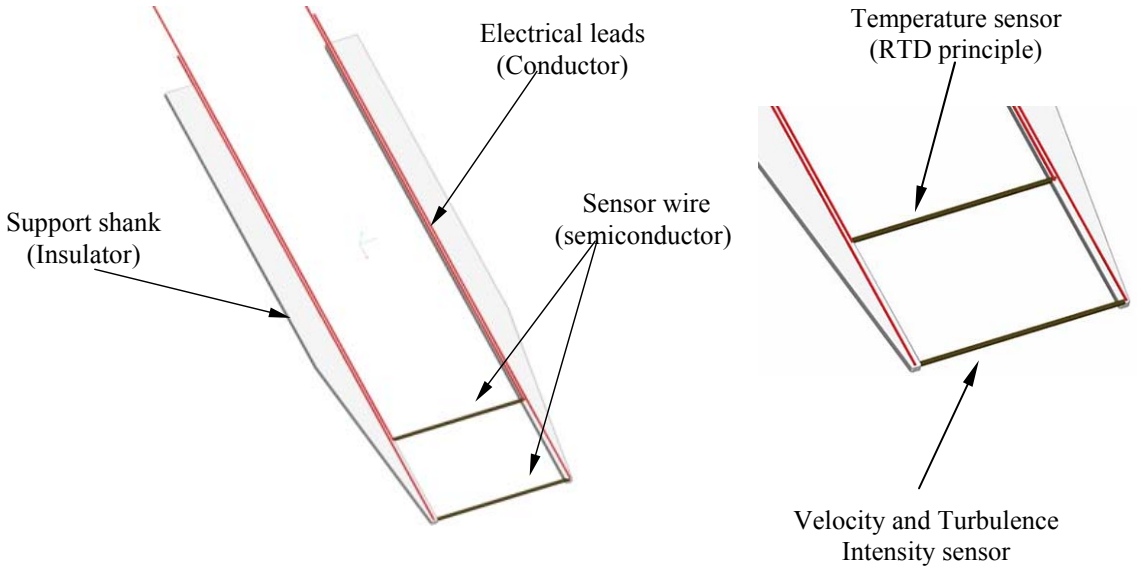

Figure 17: Constant temperature PDC-HWA with additional temperature sensor wire

4.5.2 Fabrication of PDC-HWA using microstereolithography (μSL)

The overall fabrication process of PDC-HWA can be carried out by using the cost effective microstereolithographic (μSL) technique. This technique derived from stereolithography, provides unique opportunity for fabricating complex high-aspect ratio 3D microstructures [47]. Microstereolithography is a technique that allows the manufacture of small and complex three-dimensional (3D) components in plastic material. Many of the components produced by this technique are too small and too complex to be replicated by molding and, consequently, the produced components need to have adequate mechanical or chemical characteristics to be useful. Until now, the choice of materials available in the microstereolithography process was limited to plastic, with only a few photosensitive resins available. In this study we describe new polymer/composite photosensitive resins that can be used in the microstereolithography process for manufacturing complex 3D ceramic components. During this process, their shape is unaltered, but the components undergo some shrinkage.

Research concerning the application of the microstereolithography process to ceramic / polymer composites has been successfully carried out by several research teams, and is also published in several impressive papers on the subject [47-49]. Figure 18, shows some Scanning Electron Microscopy (SEM) photos of ceramic micro structures fabricated by micro-stereolithography.

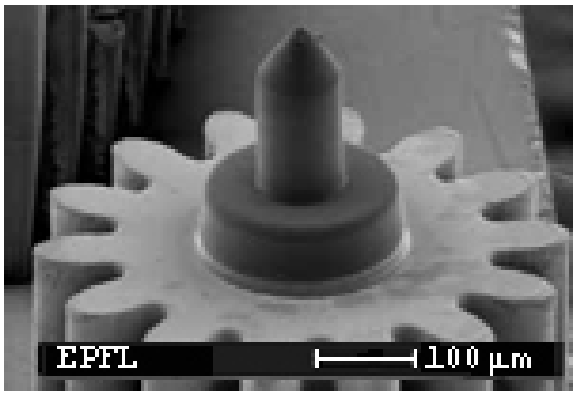

(a)

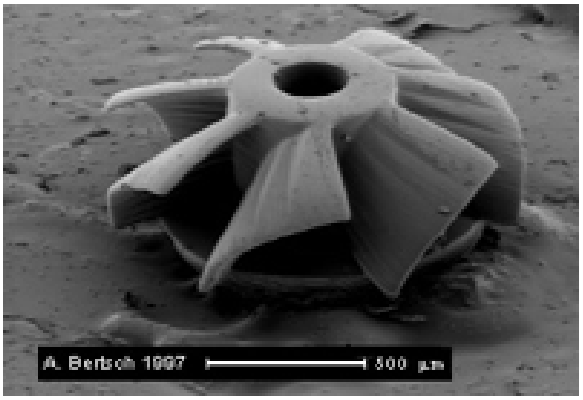

(b)

Figure 18: Scanning Electron Microscopy (SEM) photographs of a miniature (a) Gearing and (b) Turbine. (Picture Courtesy: Swiss Federal Institute of Technology, EPFL)

Figure 19 shows the photograph of Invert- micro stereolithography (I-μSL) set up. The fabrication principle is illustrated in Figure 20 schematically. The 3-D image of the component to be built is first sliced into multi-layers of 2-D images using computer software. The 2-D image is then transferred to the Dynamic Mask Generator (DMG). The ultraviolet (UV) light beam from the UV source is advanced through a series of optical systems (including mirrors and beam splitters) for changing the beam path. An adopted optical system allows to image the dynamic binary mask on the surface of the photo curable resin, with a variable magnification in order to control the size of the object [50]. The liquid polymeric precursor (resin) hardens only where touched by the light pattern. After curing, the layer will be lifted into the liquid bath and lowered to the new position to leave a certain thickness of new liquid between the bottom of the container and the first layer. Then the image of the second layer is sent to the DMG. By repeating the above steps, thin layers are sequentially solidified and stacked from top to bottom to create three-dimensional shapes, leading to 3D micro structures.

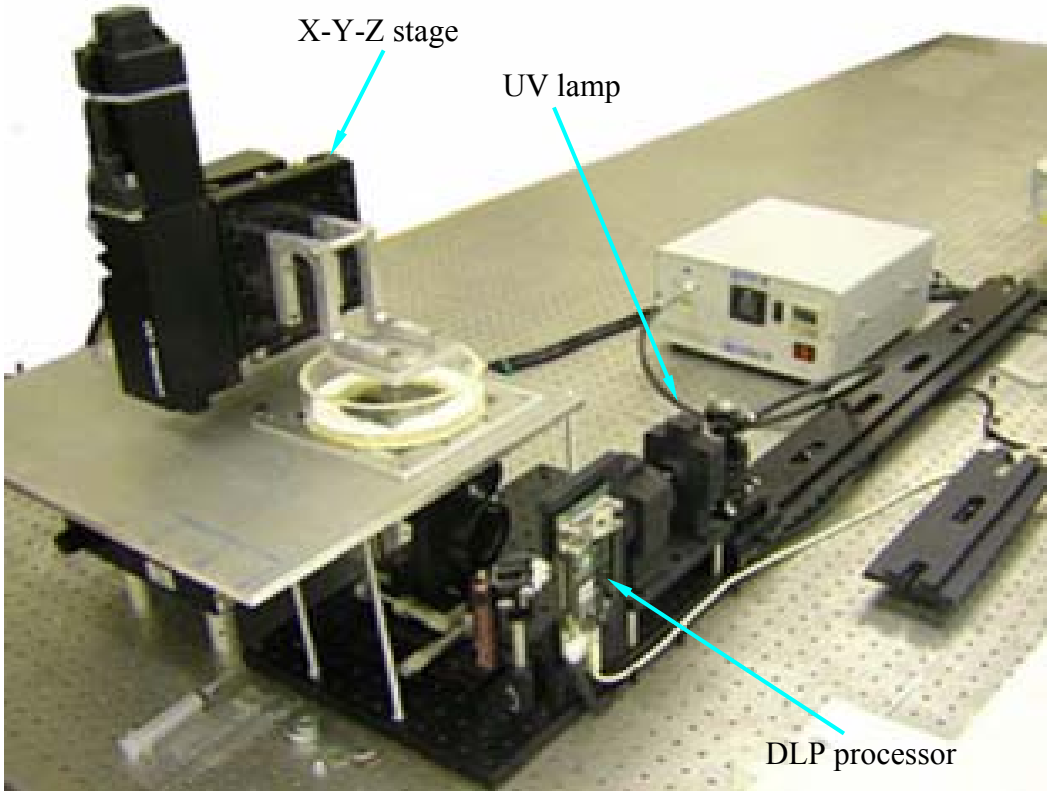

Figure 19: Photograph of Invert-micro-stereolithography developed at UCF

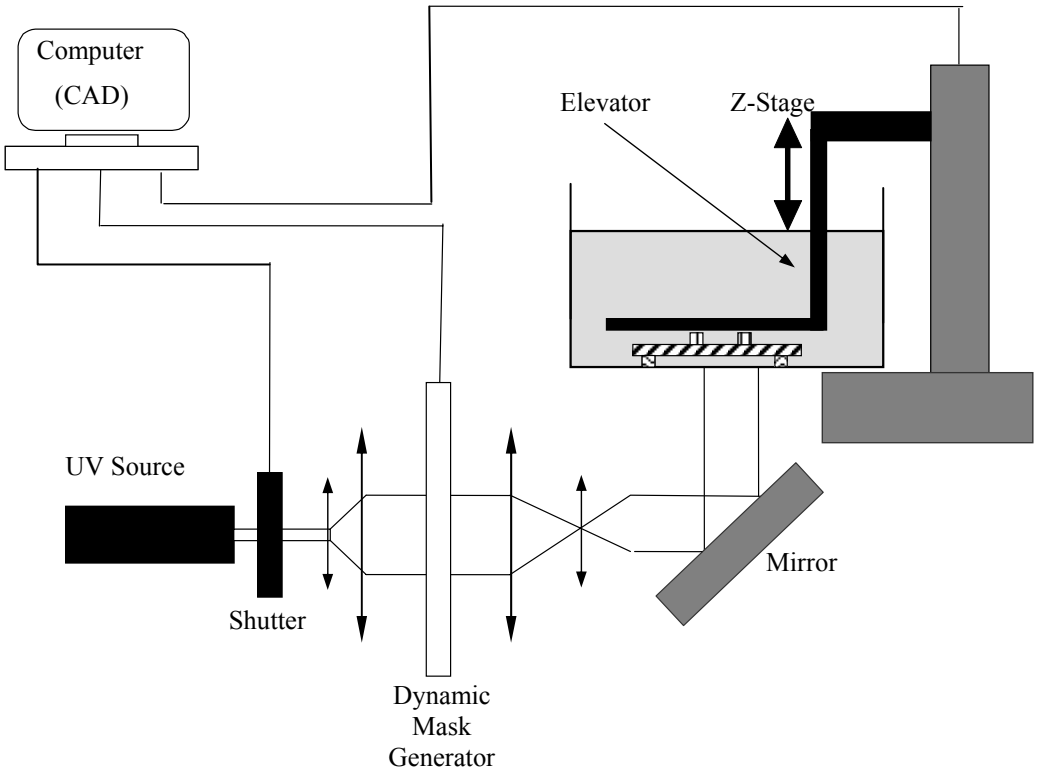

Figure 20: Principle of Invert – microstereolithography (μSL).

The first step of developing the fabrication process is to select or prepare suitable materials from the perspectives of both performance requirements and process simplicity and compatibility with the fabrication technique. As we already chose materials for different parts of the thermal anemometer, the following section explains preparation of materials/polymer precursor for fabrication in brief.

4.5.3 Materials Preparation:

The commercially available Ceraset^{TM} (from Kion Corp., USA), can be used as a UV sensitive monomer. And 2,2,-dimethoxy-2-phenyl acetophenone (commercially known as Irgacure 651 from Aldrich chemical, Milwaukee, USA), can be used as photo initiator[51].

SiCN Ceramics Precursor preparation: Precursor is prepared by adding 5_{wt}% photo initiator (Irgacure-1300 from Ciba Speciality Chemicals) to liquid Ceraset, after mixing at about 70-80^0 C for one hour, the transparent yellow liquid precursor is obtained. Then, this liquid precursor is placed in a vacuum oven at the condition of 30in Hg for 24 hours to remove air bubbles.

SiAlCN Ceramics precursor preparation: Aluminum (Al) doped SiCN ceramics precursor is prepared by mixing 5_{wt}% Aluminum isopropoxide (Alfa Aesar, Ward Hill, MA) with liquid Ceraset at 100^0 C for two hours, so that the aluminum isopropoxide can sufficiently react with Ceraset. After obtaining transparent liquid, 5_{wt}% photo initiator (Irgacure-1300) is added and stirred continually until photo initiator is dissolved fully and liquid becomes

transparent again. Then this liquid precursor is placed in a vacuum oven to remove gases bubbles and prevent oxidation.

Figure 21 is a schematic of the general fabrication process. First, the liquid precursor is spun on to a silicon wafer. The liquid thickness and, thus the final structure thickness can be varied according to the spin speed. The liquid is then subjected to non-contact UV exposure through a Dynamic Mask Generator to solidify regions of the liquid. These regions remain on the substrate while the remaining liquid is then removed by spin-rinsing in acetone solution. The result is a substrate with solid polymer structures attached. These structures are removed from the substrate. The individual structures are then crosslinked and pyrolyzed in a furnace to form PDC-MEMS devices [51].

The general Fabrication procedure for anemometer supporting prongs is shown in Figure 21 the same procedure is used to fabricate the PDC sensor wire and connecting leads separately. These PDC structures are then joined together by polymer-based bonding to form the final assembly of PDC-HWA [52]. With the description of the fabrication process of PDC complete the feasibility of the use of this PDC sensor in HWA applications

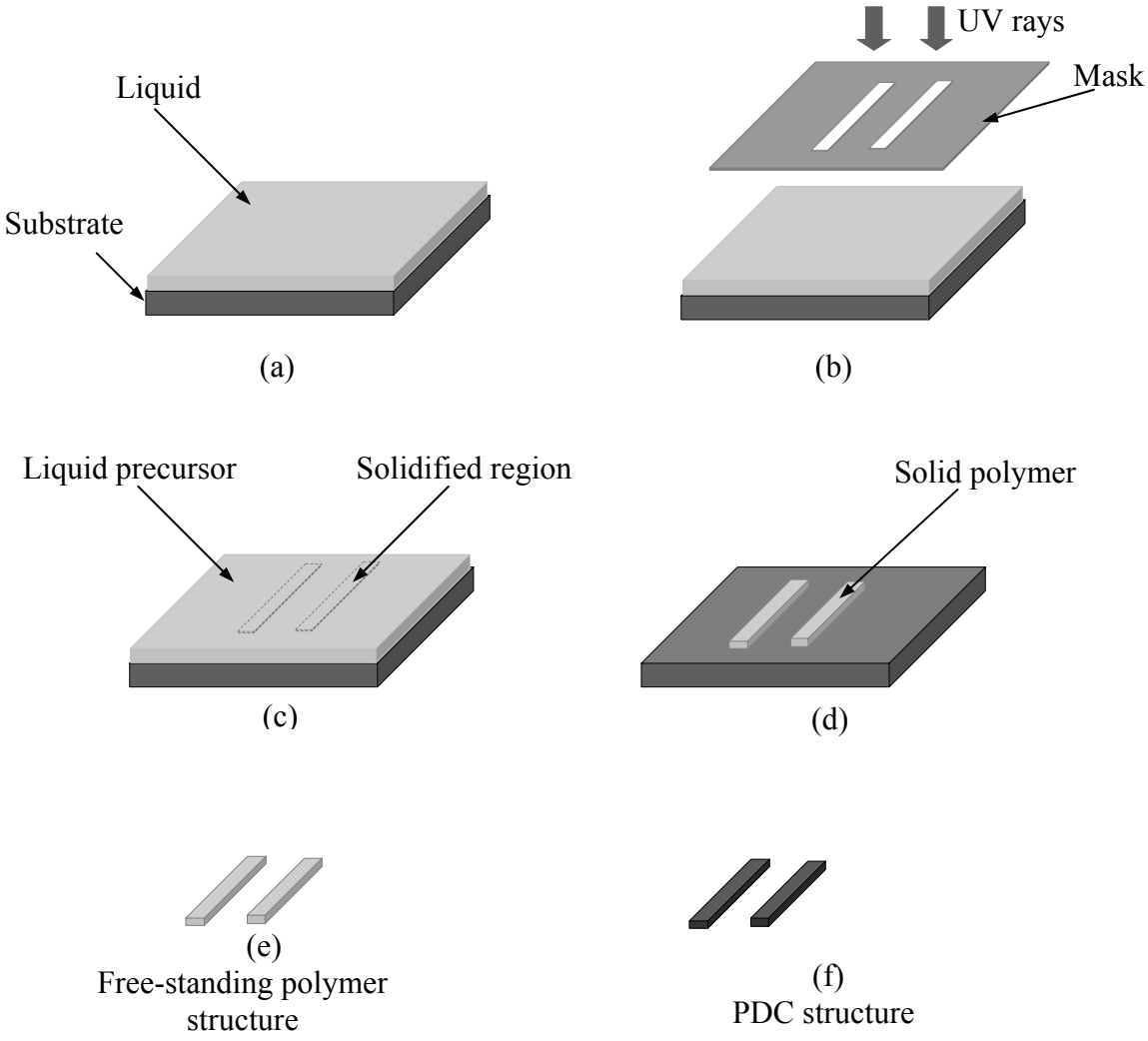

Figure 21: General Fabrication process: (a) spin precursor on to substrate; (b) UV exposure; (c) solidified polymer with remaining liquid; (d) removing non-solidified precursor; (e) remove polymer structures from substrate; (f) crosslink and pyrolyze polymer to obtain PDC structure.

4.6 Theoretical Characterization of PDC - HWA

4.6.1 Steady State Characteristics - Constant Temperature Response

Steady-state output of an infinitely long, cylindrical hot wire (large *l*/*d*) should follow King's law [9 &12]. For an HWA that has non-cylindrical geometry and smaller *l/d* ratio, we follow the common practice of collapsing the experimental hot-wire data in the form

$$P = I^2 R_s = H(U)(T_s - T_f) \tag{4.5}$$

Where T_s and T_f are the temperature of sensor and fluid respectively and R_s is the resistance of the hot-wire sensor. The H (U) term is the overall heat transfer coefficient.

$$H(U) = A_1 + B_1 U^m \tag{4.6}$$

Where *m* is a fitting factor that accounts for the smaller aspect ratio and wire geometry. The heat transfer coefficient A_1 accounts for the conduction end loss (dynamic end loss), as well as natural convection, and $B_1 U^m$ is the forced convection term [12].

The quantity of primary interest from equation 4.6 is the forced convection term; the conduction end loss term is negligible in constant temperature anemometers [53]. Rewriting equation 4.5 it can be shown that the voltage output will vary with flow speed according to the relation below:

$$\frac{V^2}{R_s} = \frac{Nu_D k_f}{D} A(T_s - T_f) \tag{4.7}$$

Where, the Nusselt number is given by:

$$Nu_D = C\,\mathrm{Re}^m\,\mathrm{Pr}^{1/3} \tag{4.8}$$

Where C=0.102 and m=0.675 are constants for noncircular cylinders in cross flow [54], k_f is thermal conductivity of fluid at film temperature $T_{film} = (T_s+T_f)/2$, Re = (ρ_fUD/μ), Pr = 0.683 at film temperature. The theoretical calibration curves for PDC hotwire as well as commercial hotwire are shown in Figure 22.

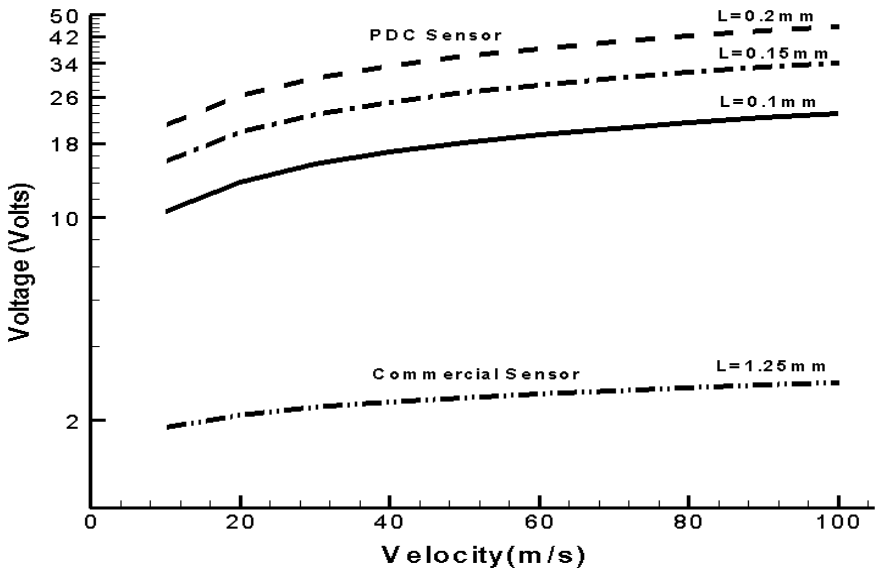

Figure 22: The steady state response of PDC hotwires of various lengths at Constant Temperature (CT) mode.

4.6.2 Frequency response

Apart from the steady state characteristics (discussed above) and directional dependence (shown later) an important element of any hot-wire anemometer system is its dynamic response.

It is a well-known fact that the HWA system operating in a Constant Temperature (CT) mode has a better frequency response when compared to the Constant Current (CC) mode of operation [10]. In the CT mode of operation, the thermal inertia of the sensor element is automatically adjusted when the flow conditions vary, by incorporating a feedback amplifier into the HWA circuit to obtain a rapid variation in the heating current to compensate for instantaneous changes in the flow velocity. Modern amplifiers have a very fast response and in the CT mode the sensor can be maintained at a constant temperature fairly effectively even for high frequency fluctuations.

The frequency response of any HWA system can be split into the response of the sensor alone and the response of the amplifier circuit. In this study the response of the proposed PDC sensor alone to the convective heat transfer from the fluid flow. Typically the sensor response follows a first order system [9, 10, and 55] and the amplitude ratio, defined by Eq. (4.9) is a function of the velocity.

$$M = \frac{1}{\sqrt{1 + (2\pi f \tau)^2}} \tag{4.9}$$

Where 'M' is the amplitude ratio, 'f' the frequency and 'τ' the time constant. The time constant is obtained from the lumped capacitance solution and given by,

$$\tau = \frac{\rho V C_p}{hA} \tag{4.10}$$

Using (4.10) in (4.9), we obtain the amplitude ratio, which is depicted as a function of frequency for various velocities in Figure 23, also shown in Figure 23, is the response of a commercial hot wire sensor.

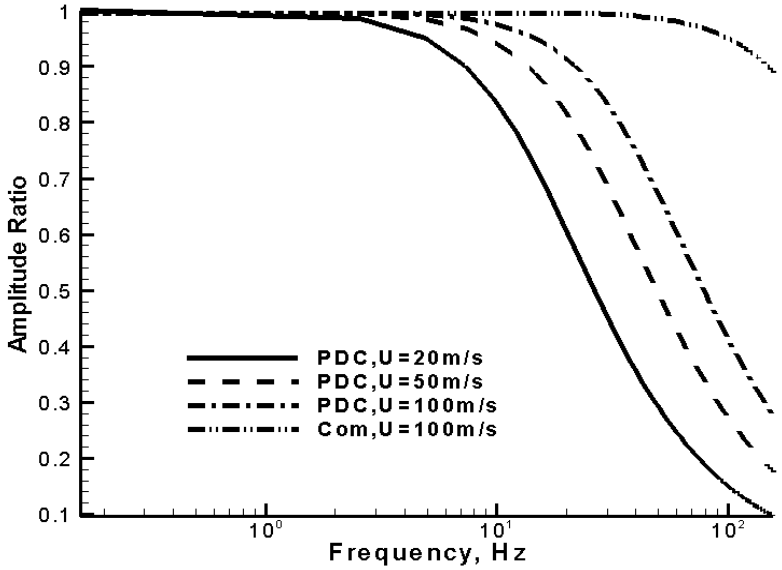

Figure 23: Frequency response in CT mode

It can be seen from the Figure 23 that for the PDC-sensor the response increases as the velocity increases. It should also be noted that this plot depicts the response of the sensor alone. The purpose of this calculation is to show the feasibility of the use of PDC as sensing elements. Suitable amplifier circuit with high frequency responses can be designed in order to form a complete PDC-HWA system, but that is beyond the scope of this investigation.

4.6.3 Directional dependence

The directional dependence of hot-wire heat transfer can be properly expressed by the effective cooling velocity or directional response equation. For hot-wire anemometers, the output characteristics depend only on two angles: yaw angle and pitch angle.

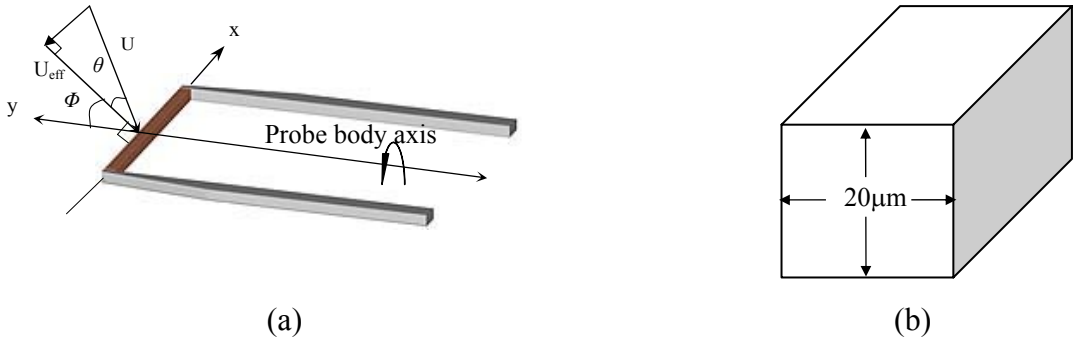

Figure 24: (a) Velocity components at sensor wire (b) Cross section of SiAlCN hot wire.

As defined in Figure 24 (a) the yaw angle θ is the angle between the velocity vector U and its transverse component normal to the wire $U_{eff,}$ and the pitch angle Φ is between U_{eff} and the hot-wire probe body axis y.

For large aspect-ratio hot wire, the yaw response should follow the cosine relation

$$U_{eff} = U\cos\theta \tag{4.11}$$

Where U_{eff} is the effective cooling velocity, which is mainly responsible for wire cooling by convection. A cosine-type response with respect to the yaw angle θ is expected. This dependence is observed as shown in Figure 25 for different velocity vector U and yaw angle θ [11].

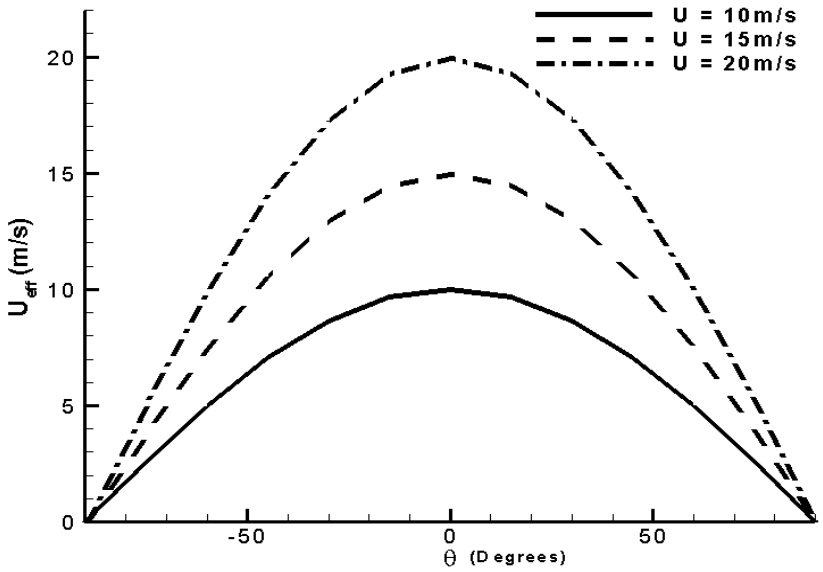

Figure 25: Yaw angle response at free stream velocity of 10, 15 and 20 m/s respectively.

Now, considering the pitch angular dependency, there are three effects that influence the outcome from the anemometer. The first one being the effect of the fluid passing through the opening formed by the wire, support prongs, and the sensor body. The additional cooling of the support shanks when they are not parallel to the flow vector, where the impact of this effect depends on the aspect ratio of the wire, causes the second effect. The third is the difference in effective cooling area of the wire caused by pitching the probe through the flow. For a conventional hot-wire with a circular cross section, this effect is absent. A ceramic (SiAlCN)

wire, which in our case implies a square cross section, will experience a difference in effective cooling area during pitching. This third effect constitutes the main difference between a conventional and ceramic (square in cross section) hot-wire sensor [14].

4.7 Structural and Thermal Analysis of PDC-HWA

4.7.1 Structural / Stress analysis:

Structural analysis attempts to estimate the maximum stress at which the proposed sensor is subjected to when examined under real engine conditions. The SiCN prongs and SiAlCN wire are used in place of conventional stainless steel prongs and platinum wire. The model was analyzed using ANSYS Finite Element (FE) based commercial code and meshed using tetrahedral elements (Solid 92). The results in Figure 26 show that the Von Mises stress of the proposed design reaches a maximum of 30 MPa.

Table 4, shows maximum allowable stress and deflection of both sensors. From these results it can be observed that the new material selection adds to a more robust sensor capable to withstand Ultra high temperature and the harsh environment to which it is exposed.

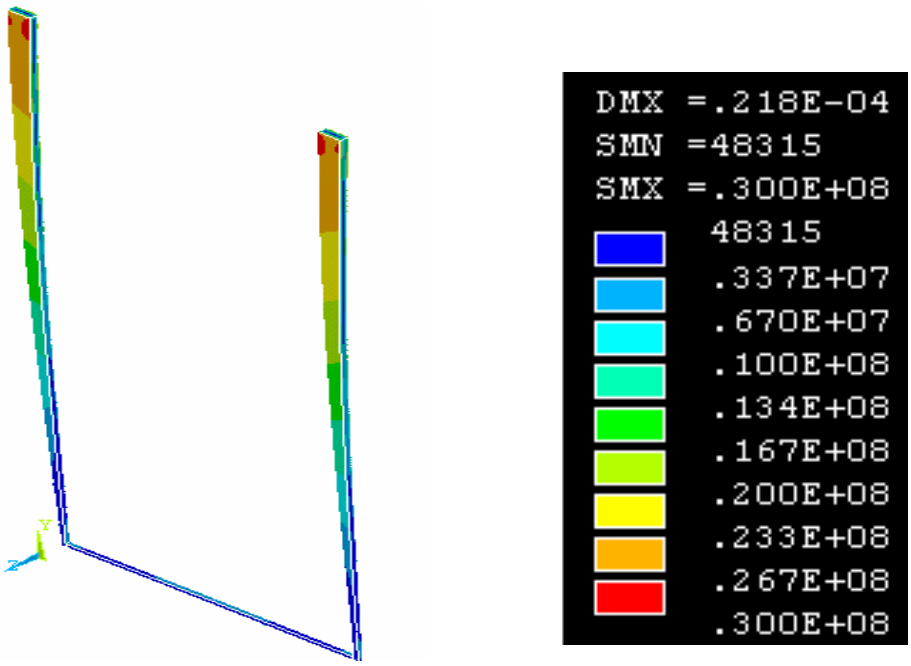

Figure 26: Contours of Von Mises stress distribution

Table 4: The quantitative measure of conduction loss

Sensor	Max. Von Mises stress (MPa)	Strength (MPa)	Yield Strength	Deflection (δ) μm
PDC-HWA	30	800	No yield	2.18
Conventional-HWA	30	480	170	25.79

4.7.2 Thermal Analysis of PDC-HWA

Estimation of Conduction loss through prongs of PDC as well as Conventional HWA

An estimation of static end conduction losses for constant temperature hot-wire sensors is given and represented in graphical form and in simple equations. End conduction heat loss for hot-wires has been considered by King [60], by Kavasznay and Toernmarck [61], Lowell [62], and more recently by Lord [63] and Ko et al. [64]. These losses were formulated for steady state conditions of the flow.

For wire geometry with small aspect ratio end conduction heat loss rate Q may contribute significantly to the total heat transfer rate $Q_{tot} = (\phi + Q)$ where ϕ is the heat transfer rate by convection from the wire [53]. End conduction losses are a consequence of the temperature gradient at both wire ends, i.e.

$$Q = 2\left(-Kw\, A \frac{\partial T}{\partial X}\right) \tag{4.12}$$

Where X is the coordinate along the wire axis with $Z = \pm\, l$ at the wire ends, T is the local wire temperature,

$$T_m = \frac{1}{2l}\int_{-l}^{l} T(z)dz \tag{4.13}$$

Is the mean temperature of the wire, and Kw is the heat conductivity of the wire.

Wire used in thermal anemometer have a non-negligible temperature co-efficient of resistance such that

$$R = R_a[1 + \alpha (T_m - T_a)] \tag{4.14}$$

Where R is the resistance of the wire, Ra is its resistance at ambient temperature and α is the temperature coefficient of wire resistivity referenced to Ta.

The heat transfer rate by convection ϕ can be expressed in terms of Nusselt number Nu as

$$\phi = \pi\ 2\ l\ k_a (T_m - T_a)\ N_u \tag{4.15}$$

Where Ka is the heat conductivity of the fluid around the sensor at film temperature Tf. Within our simple considerations, it is assumed that Nu depends on Reynolds number Re on, not on temperature loading, i.e.

$$Nu = Nu\ (Re) \tag{4.16}$$

for incompressible flow.

For static heat transfer the electrical energy supplied to the wire must equal to the heat transfer rate by convection and conduction, i.e.

$$I^2 = \phi + Q \tag{4.17}$$

Where I is the electric current through the wire.

In our computational study an estimate of static end conduction losses Q for PDC-HWA as well as conventional HWA are analyzed using FLUENT (commercial CFD package). A constant volumetric heat is generation is applied to the sensor wire. The fluid flow temperature

of 1273 K as been applied as boundary condition. A drastic decrease in conduction loss through prongs was observed when PDC material is used. Table 5 shows quantitative measure of conduction loss for both cases,

Figure 27 and Figure 28 shows the heat flux and static temperature contours obtained using FLUENT for both PDC-HWA and Platinum-HWA.

Table 5: The quantitative measure of conduction loss

Sensor	q (W) (input to wire)	ϕ (W) (through wire)	Q (W) (through 2 prongs)	% of conduction loss
PDC-HWA	0.01	0.00882	0.00106	11.44
Conventional-HWA	0.02	0.00878	0.01123	46.12

The decrease in conduction heat loss will allow most of the heat generated in the sensor wire to convect to the incoming flow, for which flow parameters needs to be determined. The decrease in conduction heat loss will increase the accuracy of the sensor, and able to measure even small variations in flow.

Table 6: Boundary conditions applied for thermal analysis of PDC - HWA

Boundary Conditions	On sensor wire	Surrounding
Temperature (^{0}C)	1200 (should be maintained)	1000
Heat transfer Coeff.-h (W/ m^2 K)	N/A	545 [@U=10 m/s] 2585 [@ U= 100 m/s]
Volumetric heat generation q```(W/m^3)	0.218 X 10^{11} [@ h = 545 W/m^2 K] 1.034 X 10^{11} [@ h = 2585 W/ m^2 K]	N/A

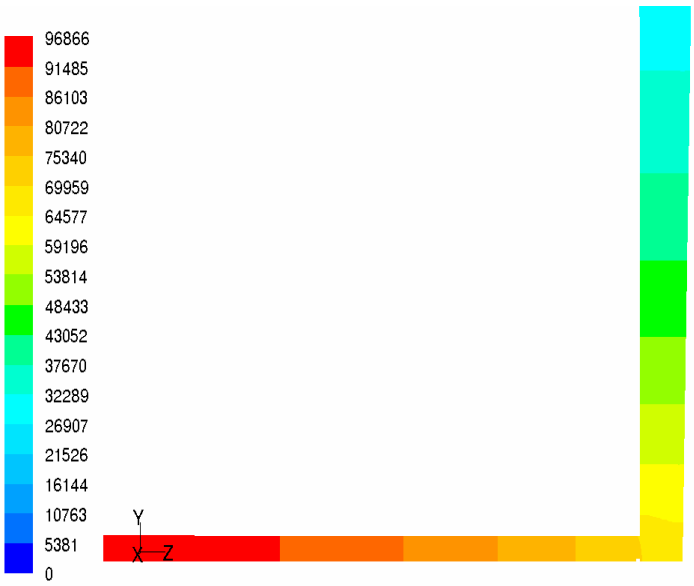

(a)

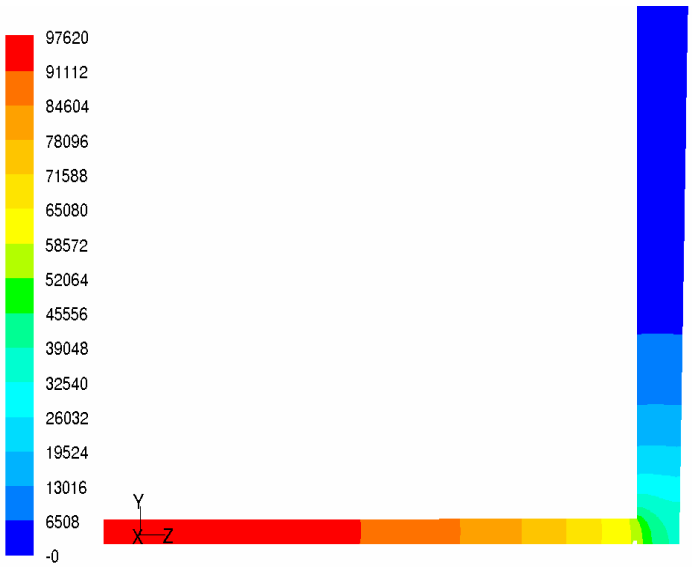

(b)

Figure 27: Contours of total-surface-heat-flux- W/m^2 (a) Platinum-HWA (b) PDC-HWA

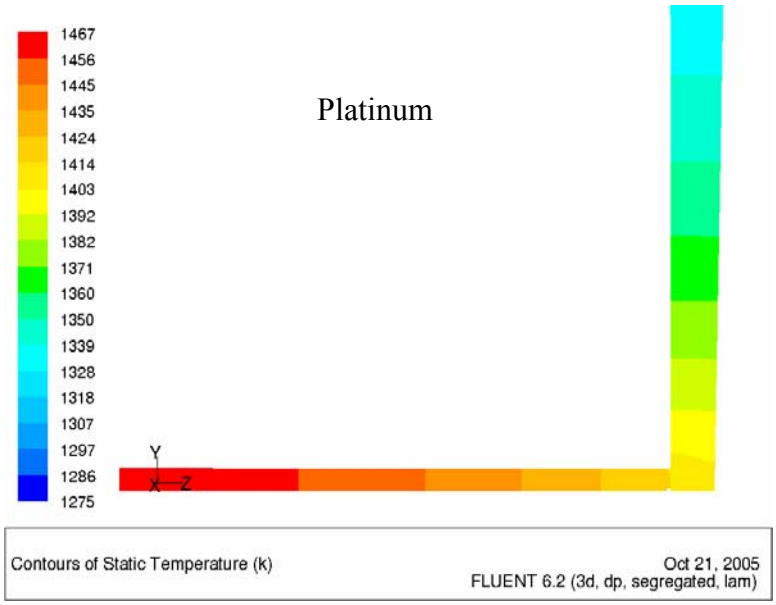

(a)

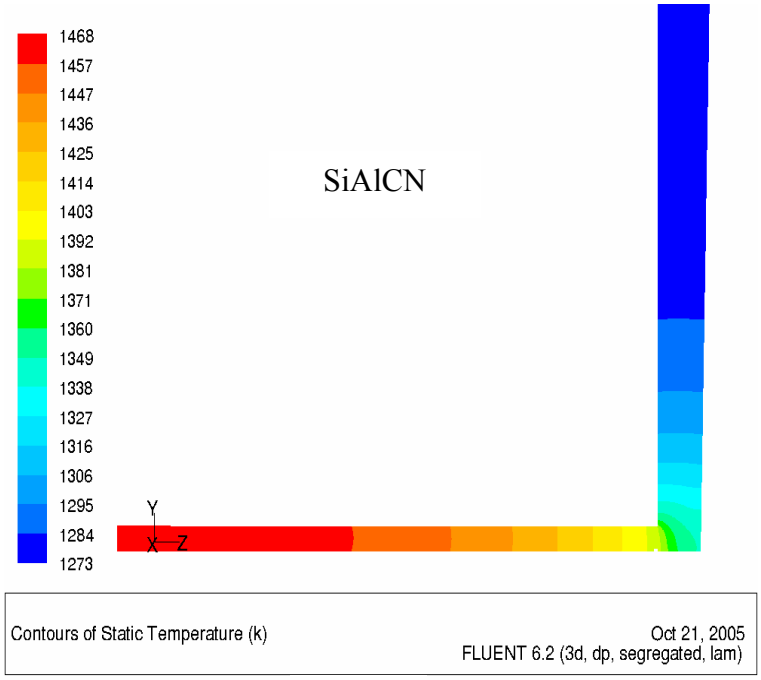

(b)

Figure 28: Static Temperature contours (a) Platinum-HWA (b) PDC-HWA

CHAPTER 5
POLYMER DERIVED CERAMIC – HEAT FLUX SENSORS

5.1. Introduction to Heat Flux Sensor (HF)

Heat flux gages are important in engineering applications where the measurement of the energy being transferred is more important than the temperature measurement. Such applications are found in turbomachinery research, building construction, and in industrial process control. Most heat flux gages are application specific. The gages are available commercially or custom made by the researchers. In spite of the numerous advances in the field of heat flux gage design, there still does not exist a heat flux gage that can perform for extended periods of time under high heat flux and high temperature conditions.

Heat flux, heat transfer per unit area, is one of the most important boundary conditions with temperature in heat transfer problems. The amount of heat flux can be evaluated by measuring the heat transfer coefficient and the wall temperature. However, it is difficult to obtain exact values of the wall temperature and the heat transfer coefficient in real situations. Thus, much research has been conducted to develop heat flux sensors which measure the heat flux without the wall temperature or the heat transfer coefficient.

Heat flux sensors are classified into three categories according to their measurement principles: the gradient method, the transient method, and the balanced method [56]. The gradient method, most frequently used, is based on Fourier's conduction law in which the heat

flux is proportional to the thermal conductivity and the temperature gradient. Gradient heat flux sensors which get the information of heat flux by measuring the temperature difference between a known thermal resistances, have two different types according to the heat flow direction; the layered gage and the circular foil gage.

5.2 Working Principle of Heat Flux Sensor (HFS):

As mentioned before heat flux sensors are classified into three categories according to their measurement principles: the gradient method, the transient method, and the balanced method. In our design of HF sensor, the gradient method is preferred for its most frequent use, and is based on Fourier's conduction law in which heat flux is proportional to the thermal conductivity and the temperature gradient.

$$Q \propto K(T)\,\frac{T_1 - T_2}{\delta} \quad (\mathrm{W/m^2}) \tag{5.1}$$

Where Q is the incident heat flux, K is the thermal conductivity of thermal resistance layer, δ is the thickness of the thermal resistance layer and $\Delta T = T_1 - T_2$ is a temperature difference measured across thermal resistance layer by RTDs.

Figure 29, shows the schematic view of the principle of the layered gage heat flux sensor in which heat flows parallel to the direction of the thermal resistance. The thicker the thermal resistance layer the larger the temperature difference and the more accurate the results.

The thinner the resistance layers the faster the response. Fast heat transfer phenomena, such as a shock wave, need a fast-response heat flux sensor, and the pursuit of the fast response is oriented to reducing the thickness of the thermal resistance layer [57, 58]. However, the reduction of the thickness of thermal resistance layer causes a reduction of the temperature difference. A thermopile, a series of thermocouples, is used to overcome the reduction of output signal caused by the thin thermal resistance layer.

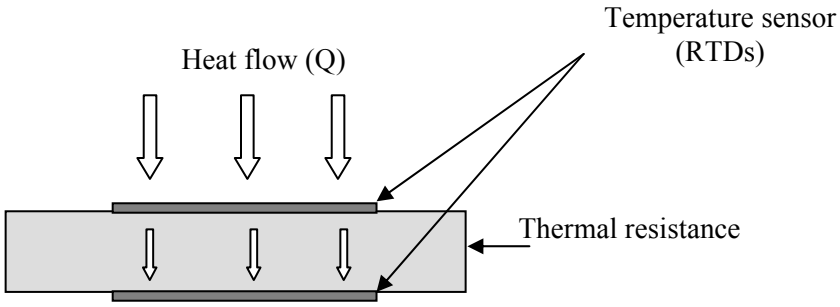

Figure 29: Principle of the layered heat flux measuring gage.

5.3 Types of Heat Flux Sensors and mounting concerns:

A heat flux sensor will invariably alter the heat flux distribution in the place where it is mounted. The idea is to minimize this disruption and still achieve a good sensor output. The exact mounting will depend on the system geometry, materials, and modes of heat transfer.

Heat flux sensors take two basic shapes/types - a flat, surface-attached, layered wafer or an insert-style cylinder. Because of its greater surface area, the surface-attached configuration is usually more sensitive than cylindrical designs. On the other hand, cylindrical sensors generally can withstand higher operating temperatures and are more easily water cooled, refer Figure 30. Also Figure 31 shows different types heat flux sensor used at present, these HFS are Intrusive type and they cannot be operative under high Heat Flux / Temperature and harsh environments.

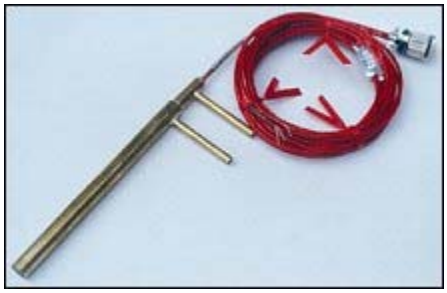

Figure 30: water-cooled Gardon gauge to withstand much higher heat flux levels.

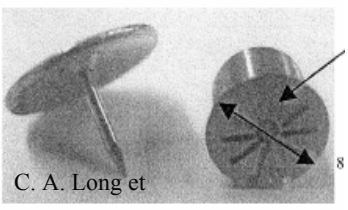

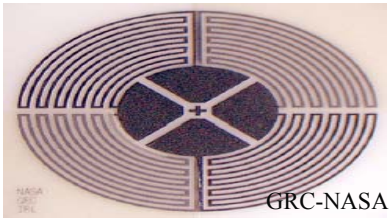

(a) (b) (c)

Figure 31: (a) Plug type HFS (b) Gardon Gauges (c) thin-film thermocouple arrays

The first issue to take into account is the thermal gradient across the sensor. If there is no thermal gradient, no heat flux will be measured. This is especially important in long duration tests in which a sensor may heat up to a uniform temperature. In these cases the sensor will probably need to be actively cooled. Because of the need for a thermal gradient, heat flux sensors do not function well if they are not mounted, because they will quickly come to a uniform or near-uniform temperature without some way to dissipate absorbed heat. This also means one must be careful mounting a heat flux sensor in a substrate with a high thermal conductivity like copper or aluminum. Such materials will have little or no thermal gradient because heat distributes itself so quickly. As a general guideline, the thermal conductivity of the sensor should be the same or larger than the material in which it is mounted for good heat flux measurements. In a well-designed sensor, thermal conductivity will be high and response will be rapid. Many heat flux sensors will therefore function well in almost any substrate but it is nevertheless important to be aware of the problems inherent in materials with high thermal conductivity. The next factor to consider is thermal contact resistance. If a heat flux sensor does not make good thermal contact with the material it is to be measuring, the sensor will cause a local hot spot to form (or a cold spot in the case where the heat flux is negative). This hot spot will alter thermal gradients and change the convective and conductive heat transfer coefficients. For this reason, cylindrical sensors are usually pressed into a substrate or held tightly into place with a mounting nut. Flat, layered sensors are usually mounted with a thermally conductive adhesive to minimize contact resistance. Simply butting a sensor against a surface may still result in a heat flux reading, but the contact resistance will keep the reading from being particularly meaningful.

The heat flux sensor disturbs the convection in a system in two ways, physically and thermally. Physically the sensor creates a discontinuity in the surface, even if it is mounted flush. The more the sensor protrudes from the surface, the greater the disruption. Thermally, the sensor alters the local temperature gradient due to its physical protrusion. The impact of the disruption the sensor causes will depend on the speed of the fluid flow. The disruption is greater for a laminar flow than for a turbulent one because of the rapidly changing, chaotic nature of the latter. The system can be considered effectively undisturbed when [59]

$$\frac{\delta k_{sensor}}{R k_{substrate}} << 1 \qquad (5.2)$$

Where

δ is the thickness of the sensor.

k_{sensor} is the thermal conductivity of the sensor.

$k_{substrate}$ is the thermal conductivity of the substrate.

R is the radius of the sensor.

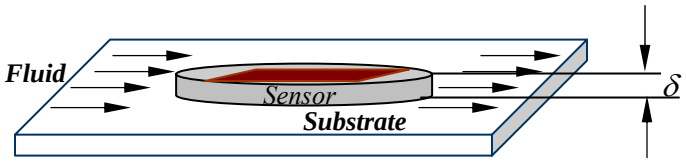

Figure 32: Sensor and substrate mounting specification.

The thermal conductivity of the PDC is significantly low; to overcome this problem we may have to install water cooling technique in the substrate to maintain temperature gradient. Or this PDC-HF sensor should be mounted on surface of which thermal conductivity is less or equal to PDC material (Example: Ceramic surfaces).

5.4 Design, Specification and Fabrication technique:

The proposed HTHF sensor consists of two Resistance Temperature Detectors (RTDs) made of SiAlCN, resistive layer made of SiCN (insulator-lightly doped) and electrical leads made of SiCN (conductor-heavily doped). The PDC materials used in our design of Heat Flux sensor not only can withstand ultra high temperature of gas turbine flow field, but also can resist contamination and oxidation (up to 1400 ^{0}C). The specifications of the sensor mainly depend on the thermal conductivity of the resistive layer. Based on thermal conductivity and required temperature gradient, the geometry of the proposed sensors, such as length, width and thickness of the sensing elements and thickness of insulating layer are shown in Figure 33 and Figure 34.

Figure 33: Side view of proposed heat flux sensor

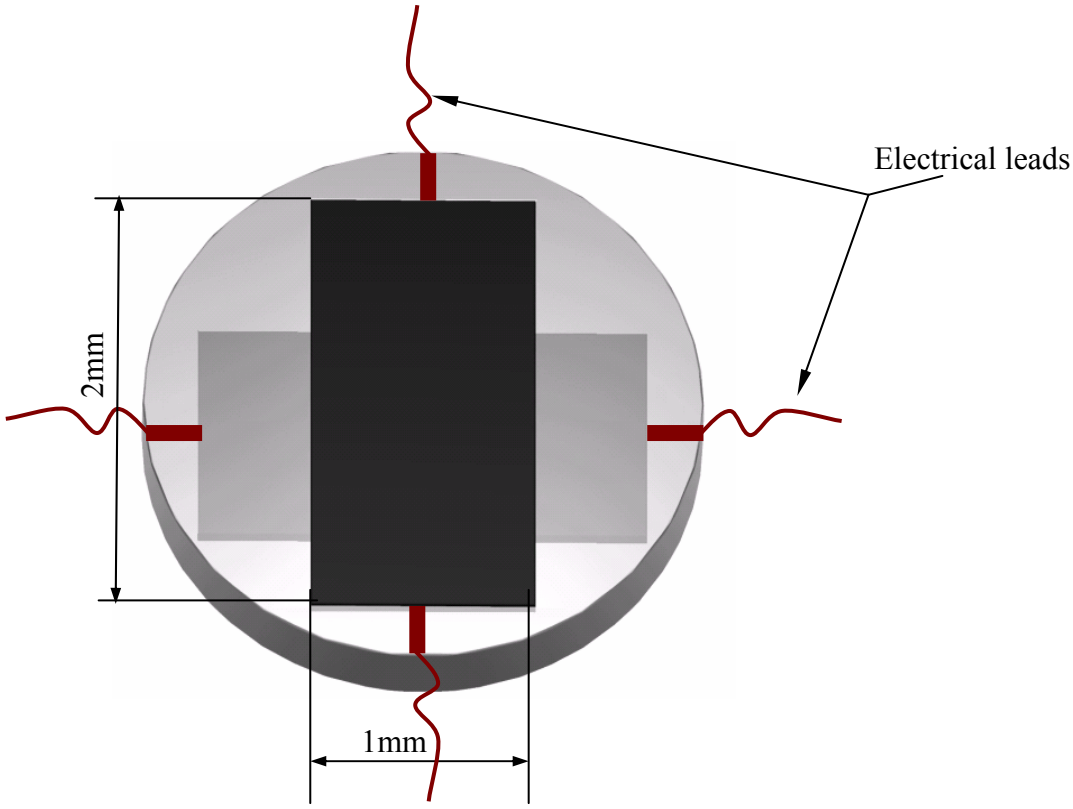

Figure 34: Schematic showing the structure of proposed temperature/heat-flux sensor.

Figure 35 shows photo-lithography process used to fabricate Heat Flux sensors, a series of deposition and etching of SiAlCN and SiCN using different mask design to fabricate final PDC-HFS which is ready to use.

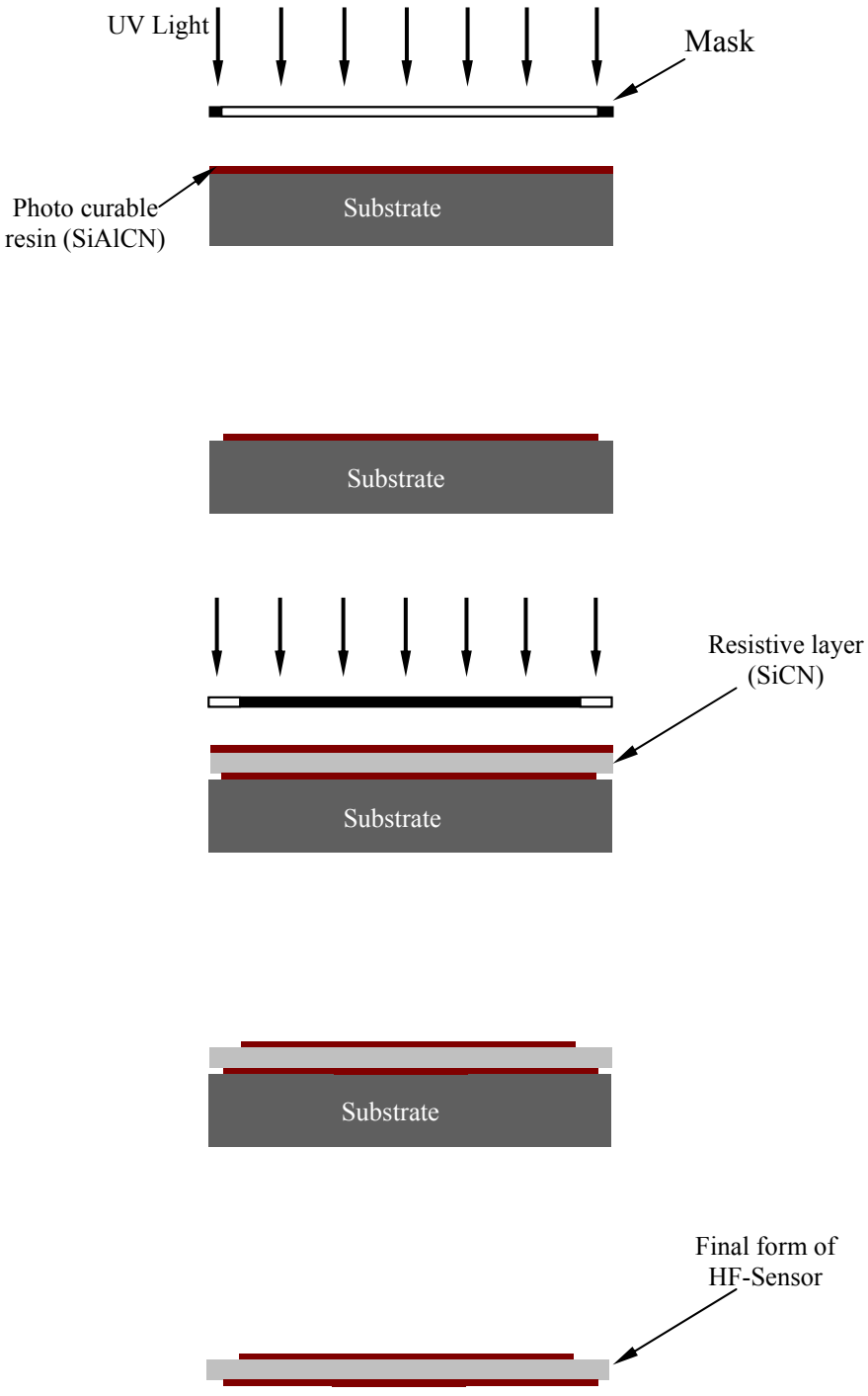

Figure 35: Fabrication of HFS by photo-lithographic technique

5.5 Thermal analysis of PDC-HFC

PDC-HFS is analyzed thermally using readily available data by K. S. Chana et al [65]. Figure 36 shows the arrangement of a QinetiQ true surface thermocouples (TST) sensor fitted to the transition duct inner wall. The thermocouple sheath was embedded into the duct wall and the bare thermocouple wires spot-welded to the inner wall. K. S. Chana et al. obtained heat rates and temperature at the transition duct in the order of 10^7 W/m^2 and 1200 K respectively. But they are not continuously monitored data; they are collected in short time. In our study of PDC-HFS these data are used as boundary condition to study the temperature and heat flux distribution. This analysis is carried out using ANSYS a finite element analysis package.

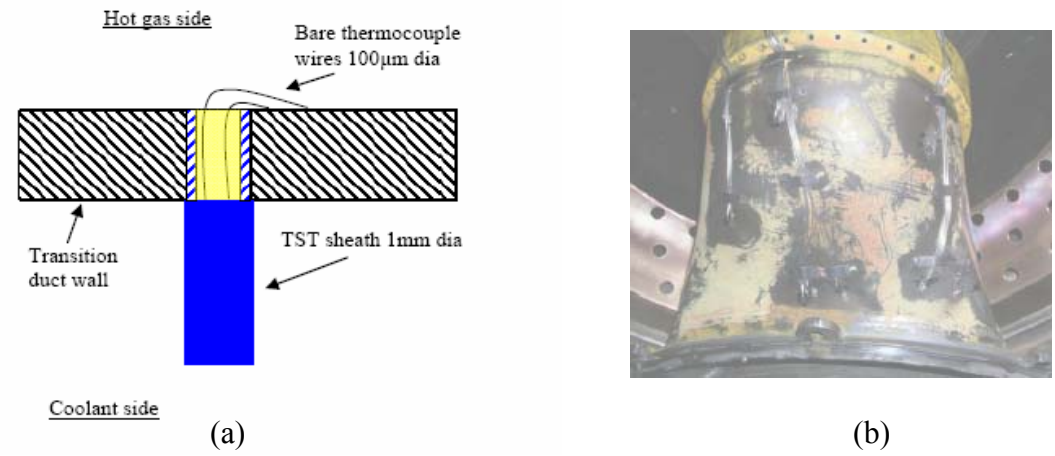

Figure 36: (a) Schematic details of True surface thermo couples (TST) & Reference thermo-couples (b) Outboard view of instrumented transition duct.

Figure 37 and Figure 38 shows 1-D temperature and heat flux distribution in PDC-HFS sensor. During thermal analysis we applied constant heat flux of $1x10^7$ W/m^2 at top surface boundary and applied constant temperature (1000 K) boundary condition at the bottom condition.

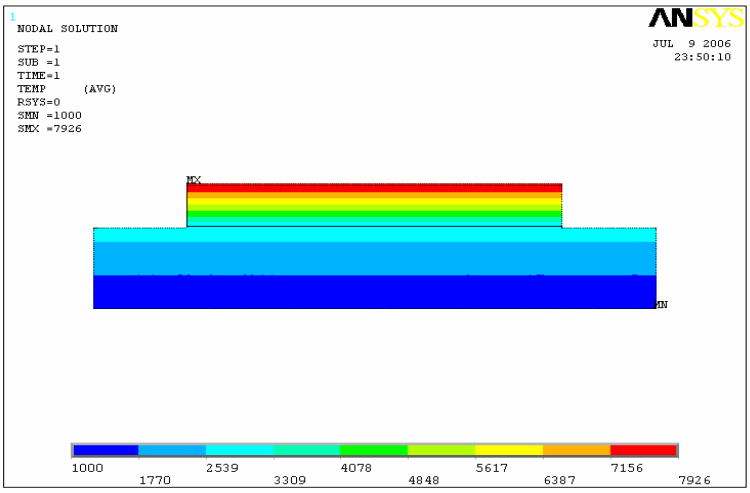

Figure 37: Temperature distribution in PDC-HFS

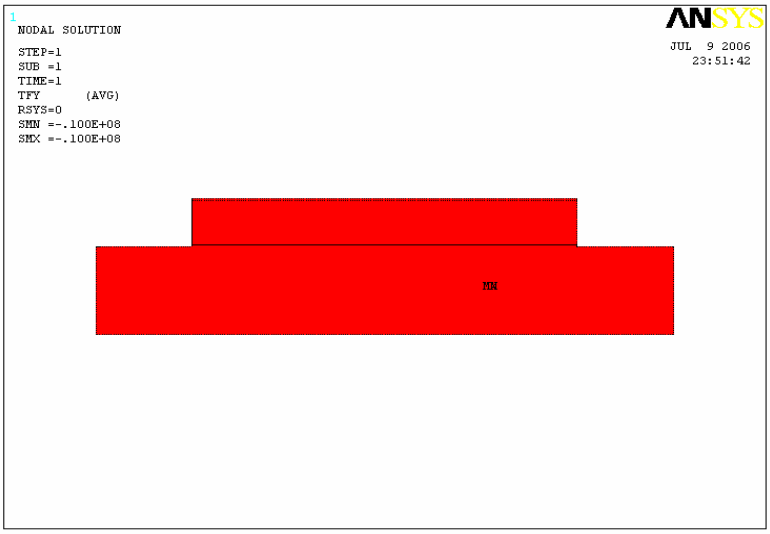

Figure 38: Heat flux distribution in PDC-HFS

CHAPTER 6
CONCLUSION

We have designed a novel PDC-HWA sensor that offer unique functional advantages over conventional hot-wire sensors. The systematic theoretical characterization of the sensor's steady state characteristics, frequency response and directional dependence has been presented. These characteristics closely follow those of the conventional hot-wire anemometers.

Our research on PDC-HWAs is motivated by the needs of fluid flow measurement in gas turbine environments. These anemometers with high tensile strength (~1000 Mpa) can outperform conventional hot-wire anemometers at ultra high temperature (~1500 ^{0}C), high turbulent flow and hostile chemical environments. The other most important advantages of these micromachined hot-wire anemometers are, their high flow sensitivity due to high specific resistivity (~$10\times10^{-2}\Omega$-m), high spatial resolution (to resolve the small eddies in a turbulent flow) and low thermal mass due to their small size.

Comprehensive optimization of design, materials and associated fabrication methods are quite involved and are not exhaustively addressed in this work. Such issues will be systematically explored to improve the performance, ease of fabrication, and reliability.

LIST OF REFERENCES

1]. Comte-Bellot, G., 1977, "*Hot-Wire and Hot-Film Anemometers*," Measurement of Unsteady Fluid Dynamic Phenomena, Hemisphere Publishing Co., pp. 123-162.

2]. Boussinesq, J., 1905, " *An Equation for the Phenomena of Heat Convection and an Estimate of the Cooling Power of Fluids,*" Journal de Mathematiques, Vol. 1, pp. 285-332, also Comptes Rendus, Vol. 133, pp. 257.

3]. King, L.V., 1914, "*On the Convection of Heat from Small Cylinders in a Stream of Fluid,*"Phil. Trans. of Roy. Soc. (London), Ser. A. Vol. 214, No. 14, pp. 373-432.

4]. Dryden, H.L., and Kuethe, A.M., 1929, "*The Measurement of Fluctuations of Air Speed by the Hot-Wire Anemometer,*" NACA-TR-320.

5]. Ziegler, M., 1934, "*The Construction of a Hot-Wire Anemometer with Linear Scale and Negligible Lag,*" Proc. K. Ned. Akad. Wet. 15,No. 1.

6]. Kovasznay, L.S.G., 1950, "*The Hot-Wire Anemometer in Supersonic Flows*," Journal of the Aeronautical Sciences, Vol. 17, No. 9, pp.565-584.

7]. Kovasznay, L.S.G., 1953, "*Turbulence in Supersonic Flow,*" Journal of the Aeronautical Sciences, Vol. 20, No. 10, pp. 657-674.

8]. Rose, W.C., and McDaid, E.P., 1976, "*Turbulence Measurement in Transonic Flow,*" Proceedings of the AIAA 9th Aerodynamic Testing Conference, Arlington, Texas.

9]. Goldstein, J., 1983, *"Fluid Mechanics Measurements"*. Hemisphere Publishing Corp. Washington, DC: pp. 99-154.

10]. Bruun, H. H., 1995, *"Hot-Wire Anemometry: Principles and Signal Analysis"*, Oxford University Press Inc., New York.

11]. Jiang, F., Tai, Y. C., Ho, C. M. and Karan, R., 1994,*"Theoretical And Experimental Studies Of Micromachined Hot-Wire Anemometers"* , Digest IEEE Int. Electron Devices Meeting (IEDM), San Fransisco: 139-142.

12]. Chen, J. and Liu, C., 2003, *"Development and Characterization of Surface Micromachined, Out-of-Plane Hot-Wire Anemometer"*. Journal of MEMS, Vol.12.

13]. Ebefors, T., Kalvesten, E., and Stemme, G., 1998, *"Three-dimensional silicon triple-hot-wire anemometer based on polyamide joints"*. IEEE Int. Workshop on Micro Electro Mechanical System (MEMS'98),.

14]. Carlsson, F., Thunblom, M., Johansson, P., Bakchinov, A., Lofdahl, L., Ebefors, T. and Stemme, G.,*"Using Silicon Based Hot-Wires for Turbulence Measurements"*. 1999, Signals, Sensors and Systems: Royal Institute of Technology, Sweden.

15]. Sherif, S. A., and Pletcher, R. H., 1999, *''An analytical procedure for predicting the response of constant ttemperature hot-wire and film anemometers''*. Journal of Measurement, Vol. 25, pp 193–201.

16]. Freymuth, P., 1979, *"Engineering estimate of heatConduction loss in constant temperature thermal sensors",* TSI Incorporated, Volume V, Issue 3.

17]. Bennethum, W. H., and Sherwood, L. T. (1998). *"Sensors for ceramic components in advanced propulsion systems"*.: summary of literature survey and concept analysis. NASA CR-180900.

18]. Paulon, J., Portat, M., Godefroy, J. C., and Szechenyi, E. (1981). *"Measurement techniques in turbomachines, ultrathin transducers applied to measurements in turbomachines"*. Measurement Techniques in Turbomachines, Vol. 2. Von Karman Institute for Fluid Dynamics, Rhode-St. Genese.

19]. Godefroy, J. C., Clery, M., Gageaut, C., Francois, D., and Portat, M. (1987). *"Sputtered alumina layers and platinel thermocouples for high temperature surface thermometers, evaluation of their electrical and mechanical characteristics"*. ONERA TP 1987-30.

20]. Wrbanek, J. D., Fralick, G. C., and Farmer, S. C., (2004). "*Development of Thin Film Ceramic Thermocouples for High Temperature Environments"*. NASA/TM-2004-213211.

21]. Long, C. A., Childs, P. R. N., Greenwood, J. R., and Tham, K. M. (2004). *"Manufacture and calibration of robust heat flux sensors for rotating turbomachinery"*. experimental Heat Transfer, Vol.17, pp.181–197.

22]. Neumann, R. D., Erbland, P. J., and Kretz, L. O. (1988). *"Instrumentation of hypersonic structures: a review of past applications and needs of the future"*. AIAA Paper No.88-2612.

23]. Kidd, C. T. (1992). *"High heat flux measurements and experimental calibrations Characterizations"*. NASA CP3161, pp. 31-50.

24]. E. Kroke, Y.L. Li, C. Konetschny, E. Lecomte, C. Fasel and R. riedel, *"Silazane Derived Ceramics and Related Materials,"* Mat. Sci. Eng.: R, 26, 97-199 (2000).

25]. R. Riedel, G. Passing, H. Schonfelder and R.J. Brook, *"Synthesis of Dense Silicon-Based Ceramics at Low-Temperatures,"* Nature, Vol.35, 714-716 (1992).

26]. R. Riedel, A. Kienzle, W. Dressler, L. Ruwisch, J. Bill and F. Aldinger, *"A Silicoboron Carbonotride Ceramics Stable to 2000 Degrees C,"* Nature, Vol.382, 796-798 (1996).

27]. K.J. Wynne and R.W. Rice, *"Ceramic via Polymer Pyrolysis,"* Annu. Rev. Mat. Sci., 14, 297 (1984).

28]. G. Pouskouleli, *"Metallorganic Compounds as Preceramic Materials, I. Non-Oxide Ceramics,"* Ceram. Int., 15, 213 (1989).

29]. M. Peuckert, T. Vahs and M. Brueck, *"Ceramic From Organometallic Polymers,"* Advanced Materials, 2, 398 (1990).

30]. L. Bharadwaj, A. Dhamne, L. An, B. Fookes, J. Kapat and L. Chow, *"Polymer-Derived Si-Al-C-N Ceramics for high Temperature Applications,"* Proceeding of IGTI ASME Turbo Expo, Jun 2003, Atlanta.

31]. L. An, Y. Wang, L. Bharadwaj, Y. Fan, L. Zhang, D. Jiang, Y. Sohn, V. Desai, J. Kapat and L. Chow, *"Silicoaluminum Carbonitride with Anomalously High resistance to Oxidation and Hot Corrosion,"* Advanced Engineering Materials, submitted

32]. L. An, R. Riedel, C. Konetachny, H.J. Kleebe and R. Raj, *"Newtonian Viscosity of Amorphous Silicon Carbonitride at High Temperature,"* Journal of American Ceramics. Soceity., 81, 1349-52 (1998).

33]. R. Riedel, L.M. Ruwisch, L. An and R. Raj, *"Amorphous Silicoboron Carbonitride Ceramics with Anomalously High Resistance to Creep,"* J. Am. Ceram. Soc., 81, 3341-3344 (1998).

34]. A. Zinmermann, A. Bauer, M. Christ, Y. Cai and F. Aldinger, *"High-Temperature Deformation of Amorphous Si-C-N and Si-B-C-N Ceramics Derived From Polymers,"* Acta. Mat., 50, 187-96 (2002).

35]. T. Hirai, K. Nihara and T. Goto, *"Oxidation of CVD Si_3N_4 at 1500^0C-1650^0C,"* J. Am. Ceram. Soc. 63, 419 (1980).

36]. P. A. Ramakrishnan, Y.T. Wang, D. Balzar, L. An, C. Haluschka, R. Riedel and A. Herman, *"Si-B-C-N Ceramics: A New Class of High Temperature, Dopable Electronic Materials,"* Applied Physics Letter**,** 78[20], 3076-78 (2001).

37]. A. M. Hermann, Y.T. Wang, P.A. Ramakrishnan, D. Balzar, L. An, C. Haluschka and R. Riedel, *"Structure and Electronic Transport Properties of Si-(B)-C-N Ceramics,"* Journal of the American Ceramic Society, 84 (10), 2260-2264 (2001).

38]. M. Scarlete, J. He, J.F. Harrod and I.S. Butler, *"Poly(methylsilane) and Poly (hydrazinomethylsilane) As Precursors for Silicon-Containing Ceramics,"* Applications of Organometallic Chemistry in The Preparation and Processing of Advanced Materials, ed J.F. Harrod and R.M. Laine, NATO ASI sereis; E: Applied Sciences vol 297, 125-140 (1995).

39]. N. F. Mott, "*Electronic Processes in Non-Crystalline Materials",* Oxford*,* 1979.

40]. L. An, W. Zhang, V.M. Bright, M.L. Dunn and R. Raj, "Proceedings of Thirteen Annual International Conference on Micro Electro Mechanical Systems" (MEMS 2000), pp 619-623(Jan 23-27 2000, Miyazaki, Japan).

41]. L. Liew, W. Zhang, V.M. Bright, L. An, M.L. Dunn and R. Raj, *"Fabrication of SiCN Ceramic MEMS Using Injectable Polymer-Precursor Technique,"* Sensors and Actuators: A. Physical, vol. 89, no. 1-2, 64-70, 2001.

42]. L. Liew, W. Zhang, L. An, S. Shah, R. Lou, Y. Liu, T. Cross, K. Anseth, V. Bright and R. Raj, *"Ceramic MEMS – New Materials, Innovative Processing and Futuristic Applications,"* Am. Ceram. Soc. Bull., 80(5), 25-30 (2001).

43]. L. Liew, Y. Liu, R. Luo, T. Cross, L, An, V.M. Bright, M.L. Dunn, J.W. Daily, R. Raj, *"Fabrication of SiCN MEMS by photopolymerization of pre-ceramic polymer,"* Sensors and Actuators: A. Physical, 95 (2-3): 120-134 (2002).

44]. Y. Liu, L. Liew, R. Lou, L. An, V.M. Bright, M.L. Dunn, J.W. Daily and R. Raj, *"Application of Microforging in SiCN MEMS Structure Fabrication,"* Sensors and Actuators: A. Physical, 95 (2-3): 143-151 (2002).

45]. C. Walsh, L. An, J.S. Kapat and L.C. Chow, *"Feasibility of a High-Temperature Polymer-Derived-Ceramic Turbine Fabricated Through Micro-Stereolithography,"* Proceeding of IGTI ASME Turbo Expo, Jun 2002, Amsterdam.

46]. J. Goldstein, 1983, *"Fluid Mechanics Measurements"*. Hemisphere Publishing Corp. Washington, DC: pp. 99-154.

47]. X. Zhang, X. Jiang, and C. Sun, 1999, "*Microstereolithography of polymeric and ceramic microstructures",* Sensors Actuators A, volume 77, PP 149–156.

48]. A. Bertsch, S. Jiguet and P. Renaud, 2004 *"Microfabrication of ceramic components by microstereolithography"*. Journal of micromechanics and microengineering, volume 14, PP 197-203.

49]. C. Sun and X. Zhang, 2002, *"The influences of the material properties on ceramic micro-stereolithography",* Sensors and Actuators A, volume 101, PP 364–370.

50]. S. J. Lee, I. H. Lee, D. W. Cho, W. Hwang, 2004,*"Design for micro-stereolithography using axiomatic approach"* Proceedings of ICAD2004, The Third International Conference on Axiomatic Design.

51]. Liew, L. A., Liu, Y., Luo, R., Cross, T., An, L., Bright, V. M., Dunn, M. L., Daily, J. W., Raj, R., 2002, "*Fabrication of SiCN MEMS by Photopolymerization of pre-ceramic polymer".* Sensors and Actuators A 95, PP 120-134.

52]. Liew, L. A., An, L., Bright, V. M., Dunn, M. L., Raj, R., 2001, "*Fabrication of SiCN ceramic MEMS using injectable polymer-precursor technique".* Sensors and Actuators A 89, PP 64-70.

53]. Freymuth, P., 1979, *"Engineering estimate of heat Conduction loss in constant temperature thermal sensors",* TSI Incorporated, Volume V, Issue 3.

54]. Incropera, F. P., DeWitt, D. P.: 2002, *"Fundamentals of Heat and Mass Transfer"*, 5 Ed., Wiley & Sons, New York.

55]. Lomas, C. G., 1986, *"Fundamentals of Hot Wire Anemometry"*, Cambridge University Press, Cambridge.

56]. Diller, T. E., 1993, *"Advances in heat flux measurements",* Adv.Heat Transfer, Vol. 23, PP. 279–368

57]. Hayashi, M., Sakrai, A and Aso, S., 1987 *"A study of a multi-layered thin film heat transfer gauge and a new method of measuring heat transfer rate with It",* Japan. Society of Aeronaut. Space Sci. Trans. Vol.30. PP. 91–101

58]. Epstein, A. H., Guenette, G. R., Norton, R. J. G., and Cao, Y., 1986 *"High-frequency response heat-flux gauge",* Rev. Sci. Instrum.Vol.57 PP 639–649

59]. Wesley, D. A., 1979. *"Thin disk on a convectively cooled plate – application to heat flux measurement errors,"* ASME Journal of Heat Transfer, Vol. 82, pp. 341-348.

60]. King, L. V., 1914. *"On the convection of heat from small cylinders in stream of fluid".* Phil. Trans. Royal Soc. London.

61]. Kovasznay, L. S. G. and Toernmark, S. I. A. "Heat losses of wires in supersonic flow, Bumblebee Series, Rep. No.127.

62]. Lowell, H. H. *"Design and application of hot-wire anemometers for steady state measurements at transonic and supersonic air speeds".* NACA TN 2117.

63]. Lord, R. G. *"Hot-wire and loss corrections in low density flows".* J. Phys. E. 7, 56-60

64]. Ko, C. L., McLaughlin, D. K., Troutt, T. R. *"Supersonic hot-wire fluctuation data analysis with a conduction end loss correction".* J. Physics. E. 11, 488-494.

65]. Chana, K. S., Syed, K. J., Wedlock, M. I., Copplestone, R. W., Cook, M. S. and Bulat, G., *" Novel unsteady temperature / heat transfer instrumentation and measurements in the presence of combustor instabilities",* ASME Turbo Expo 2005: June 6-9, 2005.